

Spring 2020

Developing a Skin Phantom for the Testing of Biowearables

Tawni Henderson

Ju Young Lee

Matthew Placide

Kiran Sutaria

Follow this and additional works at: https://scholarcommons.scu.edu/idp_senior



Part of the [Biomedical Engineering and Bioengineering Commons](#), and the [Electrical and Computer Engineering Commons](#)

Recommended Citation

Henderson, Tawni; Lee, Ju Young; Placide, Matthew; and Sutaria, Kiran, "Developing a Skin Phantom for the Testing of Biowearables" (2020). *Interdisciplinary Design Senior Theses*. 63.
https://scholarcommons.scu.edu/idp_senior/63

This Thesis is brought to you for free and open access by the Engineering Senior Theses at Scholar Commons. It has been accepted for inclusion in Interdisciplinary Design Senior Theses by an authorized administrator of Scholar Commons. For more information, please contact rscroggin@scu.edu.

SANTA CLARA UNIVERSITY

**DEPARTMENT OF BIOENGINEERING
DEPARTMENT OF ELECTRICAL ENGINEERING**

I HEREBY RECOMMEND THAT THE THESIS PREPARED
UNDER MY SUPERVISION BY

Tawni Henderson, Ju Young Lee, Matthew Placide, and Kiran Sutaria

ENTITLED

Developing a Skin Phantom for the Testing of Biowearables

BE ACCEPTED IN PARTIAL FULFILLMENT OF THE REQUIREMENTS
FOR THE DEGREE OF

**BACHELOR OF SCIENCE
IN
BIOENGINEERING
ELECTRICAL ENGINEERING**



Thesis Advisor (Dr. Prashanth Asuri)

Jun 11, 2020

date



Shoba Krishnan (Jun 15, 2020 14:03 PDT)

Thesis Advisor (Dr. Shoba Krishnan)

Jun 11, 2020

date



Shoba Krishnan (Jun 11, 2020 13:04 PDT)

Department Chair (Dr. Shoba Krishnan)

Jun 11, 2020

date



Zhiwen Jonathan Zhang (Jun 11, 2020 16:24 PDT)

Department Chair (Dr. Jonathan Zhang)

Jun 11, 2020

date

Developing a Skin Phantom for the Testing of Biowearables

By

Tawni Henderson, Ju Young Lee, Matthew Placide, and Kiran Sutaria

SENIOR DESIGN PROJECT REPORT

Submitted to
the Department of Bioengineering
and the Department of Electrical Engineering

of

SANTA CLARA UNIVERSITY

in Partial Fulfillment of the Requirements
for the degree of
Bachelor of Science in Bioengineering
and Bachelor of Science in Electrical Engineering

Santa Clara, California

Spring 2020

Developing a Skin Phantom for the Testing of Biowearables

Tawni Henderson, Ju Young Lee, Matthew Placide, Kiran Sutaria

Department of Bioengineering
Department of Electrical Engineering
2020

ABSTRACT

There is a demonstrated need in the biowearables industry for a benchtop model that can accurately emulate the perspiration mechanism and corresponding impedance vs. frequency spectra of skin. This model, or skin phantom, could increase the efficiency and accuracy of early-stage testing of biowearables, as well as minimize animal, human, and cadaver testing.

The objective of this project is to develop a skin phantom that can emulate the perspiration mechanism and impedance spectrum behavior of human skin for the testing of biowearables in the 2,000 - 20,000 Hz range. We also endeavored to create computer-simulated models to aid in the optimization of our phantom.

We designed a three-layered, PDMS-based physical model based off of the skin's sweat duct and pore structure that closely matched skin's impedance vs. frequency behavior. Our computer simulations validated our understanding of the material properties that made our phantom a good match for human skin.

While we were unable to complete all desired experiments due to campus closure, we were successful in designing and building a skin phantom that accurately mimicked the desired skin properties, while also being reusable, non-toxic, and easily manufacturable.

Further experiments should be done to validate and improve our computer simulations and mathematical models. Further manipulation of our skin phantom's factors should be done to match the skin's impedance vs. frequency behavior more closely.

Acknowledgments

We would like to acknowledge and thank the following people, without whom this project would not have been successful:

- **Jim Hutchison**, of Proteus Digital Health, who graciously loaned us a potentiostat and shared his *in-vivo* skin data with us.
- Our advisors, **Dr. Asuri**, **Dr. Krishnan**, and **Dr. Abhari**, for their guidance and mentorship.
- **Nivi Parthasarathy**, for her extensive help with the CST simulations.
- Our lab managers, **Shaun Snyder**, **Jerard Madamba**, and **Yohannes Kahsai**, for training us on lab equipment and helping us with our experiments.
- **Dr. Araci**, for his consultation on PDMS fabrication processes and for allowing us to use his Cricut Machine and his Plasma Oven.
- **Our parents**, who without their love and support, this would not have been possible.

Table of Contents

	Page
Abstract.....	iii
Acknowledgments.....	iv
Chapter 1: Project Introduction.....	1
1.1: Project Rationale.....	1
1.1.1: Problems with Current Bio-Wearable Testing Methods.....	2
1.2: Skin Phantoms.....	4
1.2.1: Existing Skin Phantoms.....	5
1.2.2: Market Needs Analysis.....	6
1.2.3: Skin Phantoms that Mimic Electrical Properties of Skin.....	7
1.2.4: Physiology of Human Skin Contributing to Impedance.....	8
1.3 Project Goal.....	11
Chapter 2: The Skin Phantom System.....	12
2.1: System Overview.....	12
2.1.1: The Physical Model Subsystem.....	13
2.1.2: The Electrical Data Collection Subsystem.....	13
2.1.3: The Circuit Model.....	13
2.1.4: The Computer Simulated Model.....	13
2.2: Integration of Subsystems.....	14
Chapter 3: Subsystem 1: The Physical Model.....	15
3.1: Overview of Subsystem.....	15
3.2: Material Choice.....	16
3.3: Fabrication.....	17
3.3.1: Flat PDMS Layers.....	18
3.3.2: Carbon Black Doped Base Layer.....	18
3.3.3: Skin Phantom Cutting and Assembly.....	19
3.4: Syringe Pump.....	20
3.4.1: Flow Rate of Salt Solution.....	20
Chapter 4: Subsystem 2: Electrical Data Collection.....	21
4.1: Overview of Subsystem.....	21
4.2: Potentiostat.....	21
4.2.1: Probe System.....	22
4.2.2: Software.....	22
4.3: Initial Testing of Potentiostat.....	23
Chapter 5: Subsystem 3: The Circuit Model.....	25
5.1: Overview of Subsystem.....	25
5.2: Data Provided by Proteus Digital Health.....	25
5.3: Early Circuit Model for Skin.....	26

5.4: Updated Circuit Model.....	27
5.5 Skin & Memristor Properties.....	28
5.6 ADS Model & Simulation.....	29
Chapter 6: Subsystem 4: Computer Simulations of the Skin Phantom.....	32
6.1: Overview of Subsystem.....	32
6.2: Baseline - “Hello World” Test.....	33
6.3 Material Simulations.....	35
6.3.1 CST Skin.....	35
6.3.2 Simplified Model of Skin - Wet Vs. Dry.....	37
6.3.3 Carbon Black + PDMS.....	40
6.3.4 PDMS.....	42
6.3.5 Simplified Model of Skin Phantom.....	43
6.4 Future Work.....	45
Chapter 7: System Integration, Testing, and Analysis.....	47
7.1: Integrating the Physical Model and Electrical Measurement System.....	47
7.1.1: Preliminary Results.....	47
7.2: Full Factorial Experiment.....	49
7.2.1: Experimental Procedure.....	50
7.2.2: Experimental Results.....	51
7.3: Analysis.....	53
7.3.1: Effects of Factors on Resistance.....	54
7.3.2: Effects of Factors on Capacitance.....	55
7.3.3: Effects of Factors on Overall Impedance vs. Frequency Behavior.....	56
7.3.4: Mathematical Model for Δ Behavior.....	59
Chapter 8: Professional Engineering Standards and Realistic Constraints	61
8.1: The Ethical Justification of Skin Phantoms.....	61
8.2: Health and Safety Implications.....	62
8.3: Sustainability as a Constraint.....	63
8.4: Civic Engagement and Compliance with Regulations.....	63
8.5: Manufacturability.....	64
8.6: Budget Constraints.....	64
8.7: Time Constraints.....	65
Chapter 9: Summary and Conclusion.....	66
9.1: Summary of the Project.....	66
9.2: Future Work.....	66
9.3 Lessons Learned.....	67
Chapter 10: Sources Cited.....	68
Appendix A: Mathematical Model for Predicting Δ Behavior.....	71
Appendix B: Budget and Actual Spending.....	72

B.1: Proposed Budget.....	72
B.2: Purchase Record.....	74
Appendix C: Timeline.....	77
C.1: Original Proposed Timeline.....	77
C.2: Actual Timeline Due to Purchasing Delays/COVID-19 Campus Closure.....	77

List of Figures

	Page
Figure 1.1: Materials Used to Simulate Skin Properties.....	5
Figure 1.2: Skin impedance from 1 Hz to 1 MHz.....	10
Figure 1.3: In-Vivo Skin Impedance vs. Frequency from Jim Hutchison.....	10
Figure 2.1: Systems Level Diagram of Skin Phantom.....	12
Figure 3.1: Simplified Perspiration model.....	15
Figure 3.2: Cross Section of Skin Phantom.....	16
Figure 3.3: Overview of Fabrication Process.....	17
Figure 3.4: Carbon Black Layer Fabrication.....	18
Figure 3.5: Bonding and Hole Punching Process.....	19
Figure 3.6: Syringe Pump Connected to the Inlet of Phantom Via Tygon Tubing.....	20
Figure 4.1: Potentiostat Schematic.....	21
Figure 4.2: Test Conditions on IviumSoft.....	23
Figure 4.3: Impedance vs. Frequency for 10 kOhm Resistor.....	24
Figure 5.1: In-Vivo Skin Impedance vs. Frequency Data from Proteus Digital Health.....	25
Figure 5.2: First Circuit Model for Skin.....	26
Figure 5.3: Simple Skin Equivalent Circuit Model from Proteus Digital Health.....	26
Figure 5.4: Impedance vs. Frequency for Simple Skin Equivalent Model.....	27
Figure 5.5: Updated Circuit Model for Skin.....	28
Figure 5.6: ADS Memristor Circuit.....	30
Figure 5.7: VSUM Node Equation.....	30
Figure 5.8: VINT Node Equation.....	30
Figure 5.9: VZ Node Equation.....	30
Figure 5.10: Memristor Hysteresis Loop.....	31
Figure 6.1: Silicon Dioxide Capacitor Simulation.....	33
Figure 6.2: Capacitance of Silicon Capacitor.....	34
Figure 6.3 : Graph of $\frac{1}{j\omega c}$	35
Figure 6.4: Bio Tissue for Bio Tissue/Skin.....	36
Figure 6.5: Impedance Vs. Frequency of Bio/Tissue Skin.....	37
Figure 6.6: Dry Skin 1mmx1mm, Fat 1mmx3mm, Muscle 1mmx5mm.....	38
Figure 6.7: Impedance Vs. Frequency of Simplified Skin Model - Dry.....	38
Figure 6.8: Wet Skin 1mmx1mm, Fat 1mmx3mm, Muscle 1mmx5mm.....	39
Figure 6.9: Impedance Vs. Frequency of Simplified Skin Model - Wet.....	39
Figure 6.10: Carbon Black + PDMS Sample With Discrete Port and PEC sheets.....	41
Figure 6.11: Impedance Vs. Frequency Graph of Carbon Black + PDMS.....	42
Figure 6.12: PDMS Sample With Discrete Port and PEC sheets.....	42
Figure 6.13: Impedance VS. Frequency Graph of PDMS.....	43
Figure 6.14: Simplified Skin Phantom Model.....	44
Figure 6.15: Real/ Imaginary Components of Impedance Vs. Frequency of Simplified Circuit.....	44
Figure 6.16: CST Model of Actual Skin Phantom.....	45
Figure 7.1: Integration of Physical Model and Electrical Measurement System.....	47
Figure 7.2: Impedance vs. Frequency for Thick and Thin Carbon Black Layers and Skin.....	48

Figure 7.3: Impedance vs. Frequency for Different Salt Solutions.....	49
Figure 7.4: Levels for Each Factor in Full Factorial Experiment.....	50
Figure 7.5: Impedance vs. Frequency for In-Vivo Skin and 32 Skin Phantom Datasets.....	52
Figure 7.6: Zoomed in Impedance vs. Frequency Curves for Full Factorial Experiment.....	53
Figure 7.7: Effect of Each Factor on Overall Resistance.....	54
Figure 7.8: Effect of Each Factor on Overall Capacitance.....	55
Figure 7.9: Zoomed in Experimental Data with Highlighted Test Cases.....	57
Figure 7.10: Formula for Δ Behavior.....	57
Figure 7.11: Effect of Each Factor on Δ Behavior.....	58
Figure 7.12: Mathematical Model for Δ Behavior.....	59
Figure 7.13: Model Predictions for Δ Behavior Against Actual Δ Behavior Values.....	60

List of Tables

	Page
Table 5.1: Skin & Memristor Properties.....	29
Table 6.1: Material Properties of Materials used in CST Simulations.....	36

1. Project Introduction

1.1 Project Rationale

Wearable medical devices are those that are attached to the body in order to diagnose or provide treatment for medical conditions and disease states. These wearable medical devices, hereafter referred to as biowearables, are becoming increasingly popular due to their ability to provide continuous, at-home monitoring and treatment [1]. As these wearable devices become more widespread, disease states can be identified and treated more efficiently than traditional methods as health care practitioners have larger and more accurate datasets to draw from than those obtained purely from office visits[1].

One popular and significant biowearable is the Continuous Glucose Monitor (CGM), which continuously monitors a patient's glucose levels throughout the day, allowing for more rapid detection of blood glucose irregularities and more efficient administration of medications to maintain safe glucose levels [2]. Another biowearable with the potential to change modern medicine is the Proteus Patch designed by Proteus Digital Health. The Proteus Patch is a biowearable sensor designed to monitor and record a patient's medication intake. Designed to be worn on the abdomen, the Proteus Patch detects when a pill has been ingested by recording and time-stamping a signal generated from a transmitter embedded within the pill[3]. The information gained from this biowearable can aid in the optimization of patient treatment, as well as ensure patient compliance with prescribed medication[4].

The increase of effective biowearables on the market has the potential to improve the way we treat certain disease states. However, a limiting factor in the development of biowearables is the testing phase, which takes considerable time and investment[5]. All medical devices require extensive testing to ensure that they interact with the point of contact in predictable and acceptable ways.

In the case of the Proteus Patch, the main interaction between the biowearable and the body is at the skin. Since the Proteus Patch is receiving a signal from within the body, the properties of

human skin affect the device's function. To ensure patient safety, the effect of the device on the skin, as well as the effect of skin on the device's system, must be known and quantified before the Proteus Patch and other biowearables that interface at the skin go to market [5]. Interactions between the Proteus Patch and human skin have caused problems maintaining electrical contact, and the perspiration of human skin can impede the patch's ability to detect the transmitter. Proteus needs to test how the patch's interaction with the skin interferes or impedes the collection of data from the transmitter in order to mitigate those effects. Improving testing of the biowearable-skin interface in terms of efficiency and accuracy will allow for a safe increase in the number of biowearables on the market.

1.1.1 Problems with Current Methods of Testing the Biowearable-Skin Interface

There are currently two types of methods to test the biowearable-skin interface: *in vivo* testing (on animals and human patients) and *in vitro testing* (using skin excised from cadavers) [6]. However, these methods are not ideal for several reasons. This section will analyze why current *in vivo* and *in vitro* methods of testing the biowearable-skin interface are problematic, as understood from both literature and from Proteus Digital Health's experience. We will then propose the use of an alternative, synthetic test subject to address these concerns. While completely cutting out animal, human, and cadaver testing in favor of a synthetic testing platform is not likely to happen at this point in time, decreasing the dependency on *in vivo* and *in vitro* tests will spare time and resources, as well as decrease ethical concerns surrounding the medical device industry.

Tests performed on animals, humans, and cadavers can be cost and time prohibitive due to difficulties in obtaining proper test subjects. Animals procured for testing need to be screened to meet certain eligibility criteria to ensure uniform testing on a standard population [7]. Additionally, costs for animal testing are rising; in 2006, European medical device companies alone spent 9.5 billion euros on animal experimentation [8]. Human patients also need to be selected carefully for the same reasons as animal subjects, but there are additional criteria involving informed consent, patient history, and safety [9]. Cadavers are especially difficult to

acquire for testing as there is a limited number available, thus demand and cost are high, not to mention the extensive regulations involved [10].

Testing early-stage medical devices on animals or humans can be highly inaccurate and misleading. Tests on animals can be inaccurate or skewed due to the effect of laboratory settings on animal psychology and skin physiology, differences in human and animal skin disease, and basic physiological and anatomical skin differences between different species [11]. Testing on humans during the early stages of medical device development can be misleading due to variations in the testing populations, especially when the skin is the area of interest; skin is inherently variable from individual to individual [6].

Perhaps most importantly, there are complex ethical issues surrounding testing medical devices on living beings. Testing medical devices on humans and animals can result in pain, injury, and death. From a utilitarian ethics standpoint, it is our ethical responsibility to minimize the amount of harm we do to other beings. While medical devices save innumerable lives, our team firmly believes that we are still responsible for minimizing the harm done in their creation. It is unlawful and unethical to test devices on humans until it can be demonstrated that there is not an undue risk of harm to the person [5]. Additionally, there are ethical concerns about using cadavers for medical research as sometimes the bodies are not obtained via body donation but because bodies go unclaimed [12].

Proteus Digital Health encountered some of these problems while performing *in-vivo* and *in-vitro* tests with their patch. First, Proteus tested the Proteus Patch on humans to understand the interactions between the skin and the patch. However, these tests proved to be cumbersome and time consuming. Since it is difficult to alter a person's skin properties, this testing could not accurately characterize interactions in different situational cases, such as prolonged sweating. Proteus also tested their patch on pigskin; however, they did not find pigskin to be an accurate model for human skin as it did not behave the same way. Using a synthetic, easily alterable

platform to test the patch on instead of a person would allow Proteus to perform tests more efficiently and accurately over a wider range of test conditions.

There is a current lack of synthetic testing methods to test the biowearable-skin interface. One emerging synthetic method of testing biowearables that would succeed in limiting *in-vivo* and *in-vitro* testing is the utilization of skin phantoms. Skin phantoms are synthetic models that emulate desired properties of skin. Such skin phantoms can be used to test specific interactions at the biowearable-skin interface.

To reiterate, the function of the Proteus Patch and other biowearables that transmit and acquire signals passing through the skin is affected by the physiological and electrical properties of human skin. A skin phantom that could accurately mimic the perspiration mechanism of skin and the corresponding impedance characteristics would aid in understanding and mitigating the adverse effects of interactions at the biowearable-skin interface. However, there aren't any existing skin phantoms that can accurately emulate these properties.

1.2 Skin Phantoms

As mentioned previously, skin phantoms, also known as 'tissue phantoms' and 'tissue-mimicking materials', are synthesized structures intended to accurately mimic desired properties of skin for use in experimental testing of biowearables [13]. Desired properties include, but are not limited to, electrical properties such as impedance, mechanical properties such as elasticity, and biological properties such as perspiration [6].

Our project aims to develop a skin phantom that meets the medical device industry's need for a synthetic platform that can accurately emulate the electrical and physiological properties of human skin. Such a skin phantom can be used in early-stage testing of wearable medical devices to minimize animal, human, and cadaver testing.

In this section, skin phantoms and their current successes and limitations will be defined in the context of testing biowearables. A market needs analysis will be discussed, and a more focused review of skin phantoms focused on those needs will follow.

1.2.1 Existing Skin Phantoms

There are currently six major classes of skin phantoms and each of these classes has specific properties that they can effectively mimic; these classes and their corresponding functions are shown in Figure 1 [6]. Although no skin phantoms that currently exist can mimic every property of skin, specific characteristics to test can be identified to inform the design and development of the skin phantom. For example, a skin phantom meant to emulate the thermal properties of skin should be composed of an elastomer, a gelatinous substance, metals, or a textile. If a skin phantom is meant to emulate electrical and optical properties, an elastomer would be a good material choice to start.

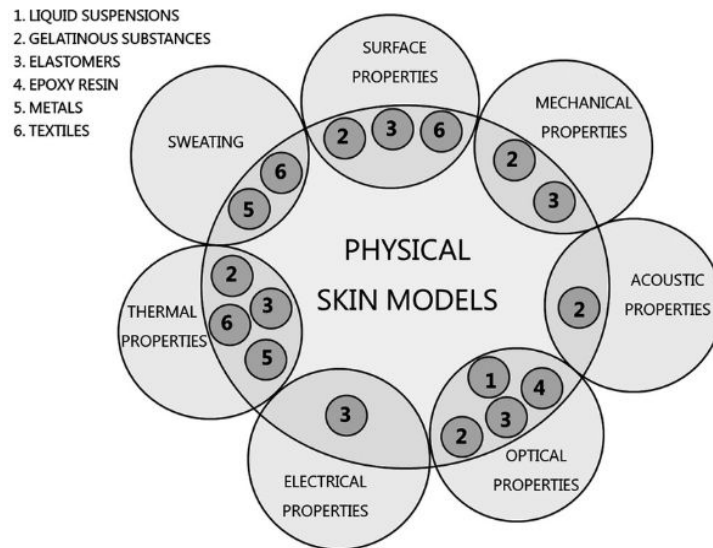


Figure 1.1: Materials Used to Simulate Skin Properties [6]

1.2.2 Market Needs Analysis

Prior to the development of a skin phantom, one must select the properties of human skin to emulate; identifying desired skin characteristics will help limit materials and other important design choices. For example, if the desired properties are electrical in nature, literature shows that elastomers are the best material to start with [6]. A market needs analysis is required to determine which qualities a skin phantom should emulate.

Through market needs analysis, we have found that there is a demonstrated need for skin phantoms in the biowearable sector; one local biowearable company that has expressed this need is Proteus Digital Health. As mentioned previously, Proteus needs to test how skin's physiological properties and impedance affect the signal acquisition of the Proteus Patch. Proteus Digital Health has developed a skin phantom for use in testing their Proteus Patch. However, they have identified several problems with their model that impedes the efficacy and accuracy of their testing process. First, their skin phantom model consists of an ion exchange membrane and a salt solution soaked sponge. These two materials are not reusable and degrade over time, meaning the phantom can only last for one day of testing. This is especially inconvenient given the materials take approximately twenty-four hours to prepare and given the materials are not cost-effective. Additionally, the same phantom cannot be used to test multiple experimental setups as the phantom cannot be altered once it has been assembled.

Proteus has indicated a need for a skin phantom that mimics the impedance vs. frequency spectra of human skin while also demonstrating longevity, cost-effectiveness, and easy customizability. Additionally, the number of skin phantoms in development that are intended to mimic either the impedance or perspiration mechanism of skin suggest that there is a wider need for this kind of skin phantom in the biowearable industry beyond Proteus Digital Health. These developing skin phantoms and their shortcomings will be discussed in the following sections.

Thus, we have decided to focus our project on developing a skin phantom that meets the needs of the biowearable industry. As noted previously, a skin phantom's materials and method of

fabrication are determined by the characteristics one wishes to emulate. Since we have identified our desired characteristics as the impedance of skin, we can begin designing our phantom based on currently existing skin phantoms with those same properties.

1.2.3 Skin Phantoms that Mimic Electrical Properties of Skin

With a more narrowed scope, a more focused literature search can be performed. There are several existing skin phantoms that seek to mimic the electrical properties of human skin, with limited success. Exploring and analyzing the successes and failures of these phantoms will guide the development of a new skin phantom.

One existing skin phantom that mimics impedance was developed by Pinto, Bertemes-Filho, and Paterno. Their phantom was made of gelatin, salt, and formaldehyde. By varying the amount of salt in their phantom, Pinto, Bertemes-Filho, and Paterno were able to mimic the impedance of skin on various parts of the body, such as the pectorals and wrist [14]. While this skin phantom was largely successful, there are a couple of drawbacks to this approach. First, the materials used in this model present some concerns. Formaldehyde is a very toxic substance and must be handled with care [15]. Gelatin degrades over time, though the process is slower if the gelatin is cross-linked with formaldehyde [16]. The degradation of the gelatin means that this skin phantom has a limited lifespan as the material properties will change over time. The second drawback to this type of phantom is the difficulty in changing the experimental setup. In order to mimic different parts of the body, an entirely new phantom needs to be created as the salt concentration can only be determined prior to the gelatin being crosslinked. This phantom has demonstrated the importance of material selection.

As noted previously, many skin phantoms that emulate the electrical properties of skin are made of elastomers [6]. One elastomer that is commonly used for skin phantoms is polydimethylsiloxane (PDMS). PDMS makes a good base for a skin phantom because it is long-lasting, easy to shape, and nontoxic [6]. However, PDMS is not conductive; it has a very high impedance and needs to be altered in order to pass an electrical signal through it [17]. One

way that PDMS can be made conductive is by doping it with carbon black powder [18]. Additionally, PDMS is a desirable material for skin phantoms due to its longevity, manufacturability, biocompatibility, and alterability [19,20].

While there are several existing phantoms that are composed of PDMS and carbon black doped PDMS, there are none that have the same functionality we are looking to create with our skin phantom. Nonetheless, analysis of these phantoms will aid us in understanding the material we have chosen to use for our phantom, as well as help us anticipate and solve problems we may encounter.

One existing PDMS skin phantom is one developed by Guraliuc, Zhadobov, and Sauleau that is intended for wave propagation studies in the 60 GHz range [21]. In order to make their phantom conductive, they doped PDMS with carbon black at various concentrations, finding that the higher the concentration of carbon black, the higher the conductivity of the phantom. However, adding too much carbon black began to cause unequal distributions and clumps of carbon black in the PDMS [21].

The phantoms we have discussed thus far have replicated skin properties by relying mostly on material properties of chosen substrates rather than the actual mechanisms which produce those traits in human skin. As those phantoms have not completely succeeded in their goal, our group decided to base our mechanisms on the actual physiology of human skin; particularly those aspects of physiology that contribute to skin impedance. Thus, a review of human skin physiology is needed.

1.2.4 Physiology of Human Skin Contributing to Impedance

In order to create a skin phantom that mimics skin impedance, we must understand the aspects of skin physiology that determine its impedance. Skin impedance varies with respect to the frequency of the applied signal, so it is important to determine what frequency range we want our skin phantom to operate under [22]. The Proteus Patch and Transmitter operate in the

10,000-20,000 Hz range. Thus, we will design our phantom to mimic skin impedance in the 2,000 -20,000 Hz range; this is wider than the range the Proteus Patch operates under as we want our phantom to be useful to other companies as well.

Skin impedance is determined by water content and sweat; the more hydrated skin is, the lower the impedance [22, 23]. Skin hydration, sweat rates, and sweat ionic concentration vary from person to person, meaning that skin impedance is highly variable from person to person, so it will be necessary to have a skin phantom that is easily adaptable to account for this [24].

Additionally, sweating rates are different in different parts of the body; while we intend for our phantom to be variable in order to account for this, we are choosing to focus our initial studies on sweat rates of the abdomen, as that is where the Proteus Patch is worn [25]. The sweating rate of abdominal areas ranges from 1.2 - 11 g/m² per hour; this is a wide range as it accounts for variations between different people and ages [25, 26]. The average salt concentration of sweat falls in the range of 20-60 mmol/L [24].

Sweating and skin hydration are the main determinants of human skin impedance; therefore, we intend to create a skin phantom that mimics this physiological phenomenon in order to replicate human skin impedance. Creating a skin phantom more accurate to human physiology will allow us to easily mimic the inter- and intra-personal impedance vs. frequency seen in actual human skin.

There are two sets of data for skin impedance vs. frequency; one is shown below in Figure 1.2 and comes from a study published in 1988 by Pallas-Areny, Ramon, Riu, and Pere [27]. The second set is shown in Figure 1.3 and was generously given to us by Proteus Digital Health. Our project mentor at Proteus collected this data from his own skin with the same potentiostat loaned to us.

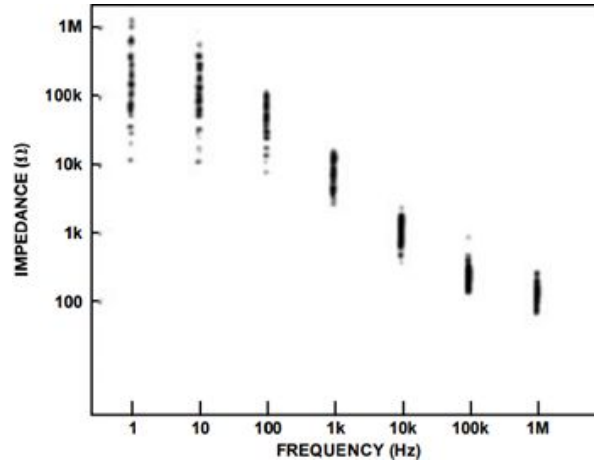


Figure 1.2: Skin impedance from 1 Hz to 1 MHz [26]

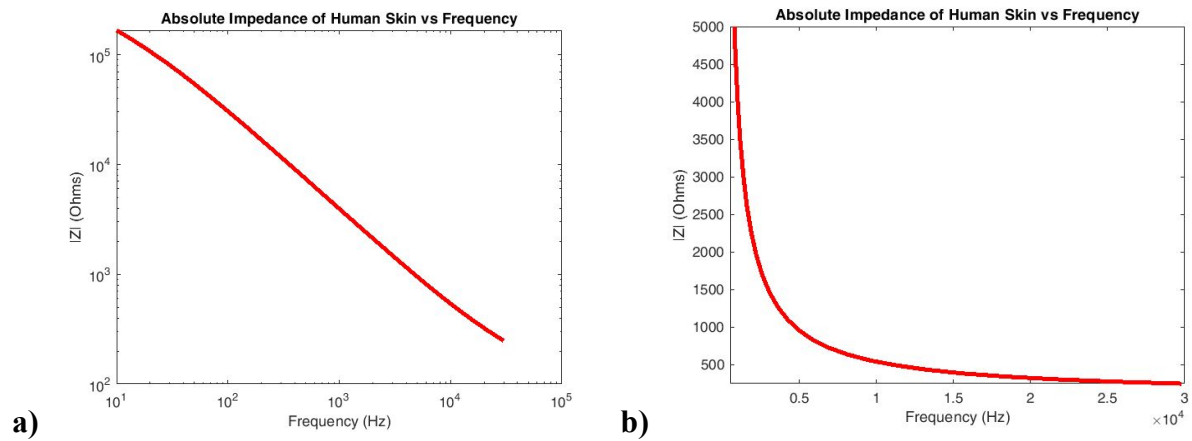


Figure 1.3: In-Vivo Skin Impedance vs. Frequency from Jim Hutchison

a) Logarithmic Scale b) Linear Scale

Figures 1.2 and 1.3 demonstrate that while impedance vs. frequency may differ from person to person, it largely maintains the same behavior. Thus, our phantom should be designed to mimic skin's impedance vs. frequency behavior, but not magnitude as that can vary from person to person. We will use Jim Hutchison's data as our benchmark as it was collected using the same instrument we will use during testing.

1.3 Project Goal

The biowearable device industry has demonstrated a need for a skin phantom that accurately mimics human skin perspiration and its corresponding impedance vs. frequency behavior. Our project aims to create a skin phantom that not only meets that need, but also demonstrates longevity, ease of manufacturability and customization, cost-effectiveness, and reusability. In order to meet these qualifications, our skin phantom will be a fluidic system composed of PDMS and carbon black that emulates the physiological phenomenon of sweating. We also aim to create a circuit model for skin and computer simulation of our physical skin phantom. As we want our phantom to be customizable, simulations will aid the end-user in determining the best parameters for their phantom to meet their desired behavior.

2. The Skin Phantom System

2.1 System Overview

As mentioned in the previous section, we are designing a skin phantom that can mimic the skin's perspiration mechanism and corresponding impedance spectrum for the testing of biowearables. Our skin phantom system is composed of four subsystems: the Physical Model, Electrical Measurement System, the Circuit Model, and the Computer Simulated Model. A diagram of these four subsystems is summarized in Figure 2.1.

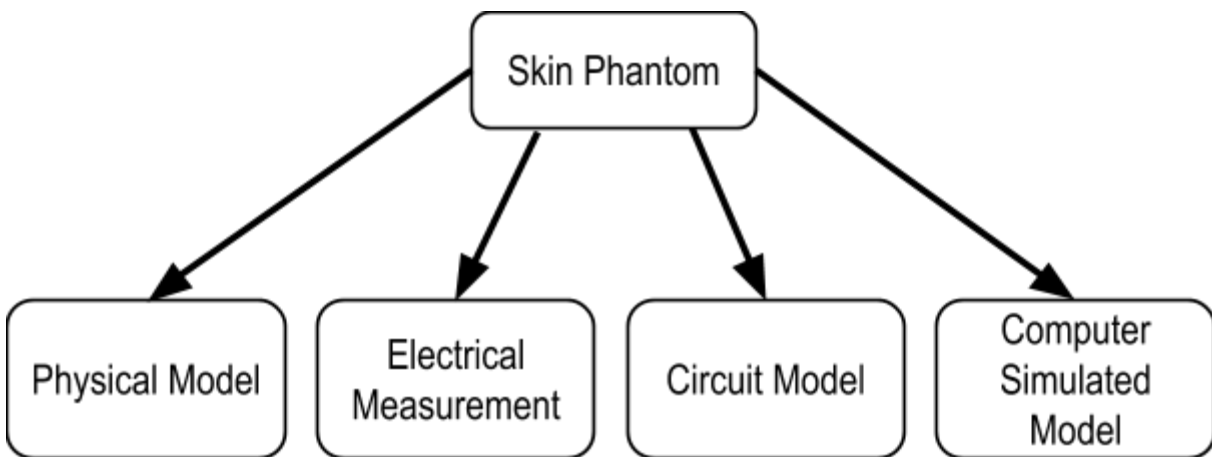


Figure 2.1: Systems Level Diagram of Skin Phantom

2.1.1 The Physical Model Subsystem

The Physical Model Subsystem is the most unique subsystem of the skin phantom system. This subsystem is the part of the device that mimics the impedance spectra of skin and will be directly measured for impedance over a frequency range of 2,000-20,000 Hz. We decided to use an elastomer as the base of our phantom as our literature review demonstrated skin phantoms made of elastomers were the best suited for mimicking the electrical properties of the skin.

Furthermore, in keeping with our goals of creating a long-lasting phantom, we chose PDMS to be the primary material. PDMS is desirable due to its longevity, manufacturability, biocompatibility, and alterability. In order to mimic the biological properties of sweat, a syringe pump was connected to pump a conductive salt solution through channels and pores in the

elastomer. This subsystem will be further explored and explained in Chapter 3: The Physical Model.

2.1.2 The Electrical Data Collection Subsystem

The Electrical Data Collection Subsystem consists of a potentiostat and a computer with associated software to collect and analyze the data. Our potentiostat, an Ivium Vertex with Electrical Impedance Spectroscopy (EIS) capabilities, was generously loaned to us by Jim Hutchison at Proteus Digital Health. We used the associated IviumSoft software to collect and export the impedance data. This subsystem will be further explored in Chapter 4: Electrical Data Collection.

2.1.3 The Circuit Model

The Circuit Model was developed in order to model the skin's behavior using circuit elements. While there are circuit models for skin that only use traditional circuit elements such as resistors and capacitors, they do not accurately represent the skin's nonlinear behavior. Thus, a model consisting of memductors and memristors was created. This subsystem will be further explored in Chapter 5: The Circuit Model.

2.1.4 The Computer Simulated Model

The Computer Simulated Model consists of simulations all designed and completed on Computer Simulation Technology Studio Suite®. The initial purpose of the simulations was to determine which factors and materials produced the best phantom that accurately mimicked our expected impedance vs. frequency curve. This subsystem also provided data that confirmed the expected impedance versus frequency behavior of human skin, a simplified model of the human body (skin, muscle, fat), carbon black mixed into polydimethylsiloxane (PDMS), PDMS alone, and a simplified model of our skin phantom. This subsystem will be further explored and explained in Chapter 6: The Computer Simulated Model.

2.2 Integration of Subsystems

The four subsystems will be integrated in such a way that they aid the performance of the other subsystems. The electrical measurement system will be used to collect and analyze data from the physical model. The computer simulations will initially validate our choices of materials for the physical model, based both on the literature research of the electrical properties of skin, as well as the developed circuit model for skin. Then, once the electrical measurement system is integrated with the physical model, computer simulations will be made to simulate our actual model and its measured behavior. This will inform further iterations of the physical model by helping to optimize different parameters.

3. Subsystem 1: The Physical Model

3.1 Overview of Subsystem

The Skin Phantom subsystem is the most critical part of the overall system as it is the component that mimics the physiological and electrical properties of the skin. As mentioned in Chapter 1, the impedance characteristics of the skin are primarily determined by water content in the skin. As such, we designed this subsystem to mimic the sweat duct and pore physiology of the skin, as seen in Figure 3.1. This biomimicry approach was taken to increase the accuracy of our phantom, as function follows form.

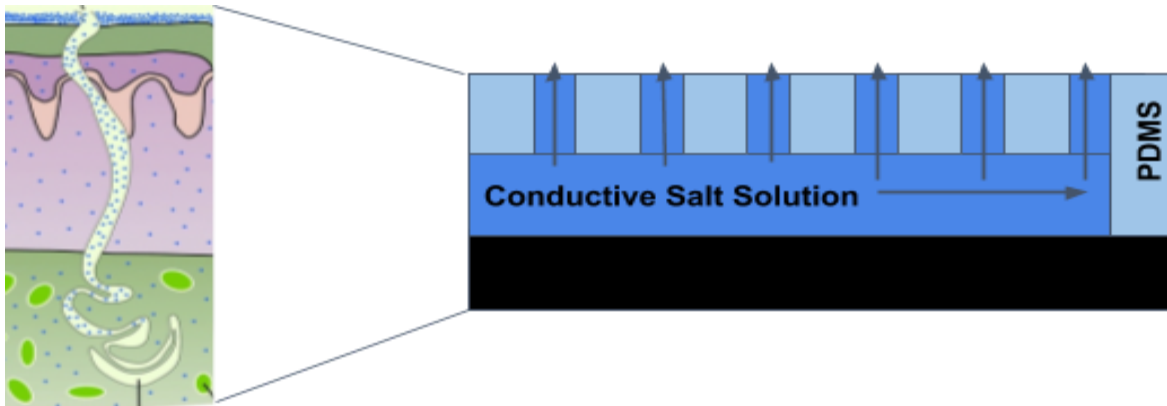


Figure 3.1: Simplified Perspiration model

From this simplified perspiration model, we developed a three-layered structure, shown in Figure 3.2, that would allow for a conductive salt solution (mimicking sweat) to flow through the structure and up through pores.

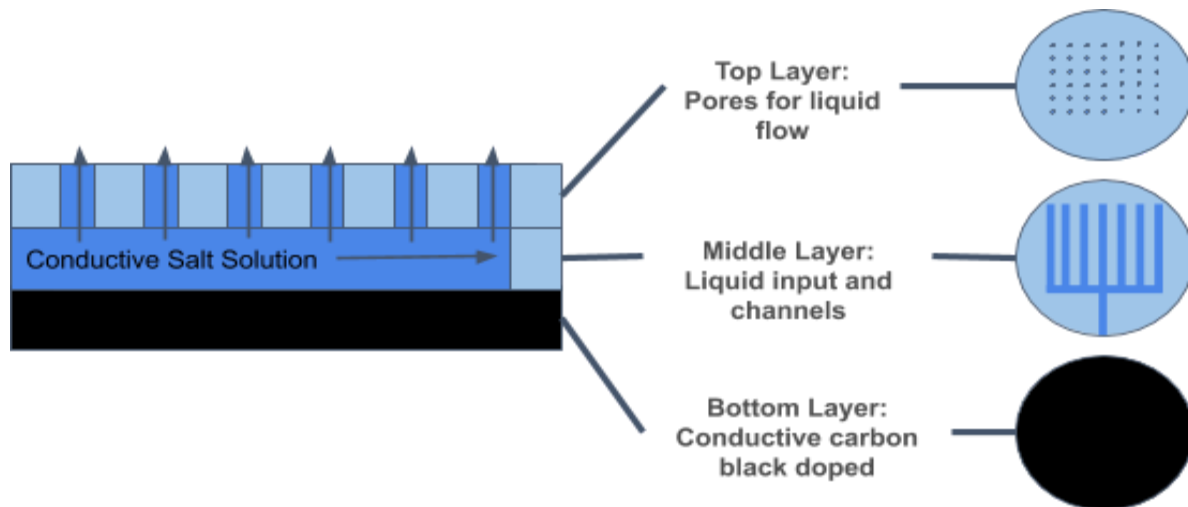


Figure 3.2: Cross Section of Skin Phantom

The electrical properties of our phantom are dictated by the conductive solution in the channels and the composition of the bottom layer. While these features individually are not unique to our phantom, our approach of mimicking skin physiology to influence electrical properties is novel. The advantage of using this novel approach is the ability to change the electrical properties of our phantom without needing to fabricate a new phantom. We chose to make our phantom in layers for ease of fabrication, simplicity, and cost-efficiency.

3.2 Material Choice

Our project goal includes making our phantom durable, inexpensive, non-toxic, and easy to fabricate in order to fulfill needs that are not all met in many contemporary phantoms. Additionally, our design is made to mimic biological skin and the act of sweating, which split the skin phantom into two parts: a solid part which is flexible and nonconductive and a liquid part that provides electrical properties.

These design constraints made elastomeric materials favorable for the solid portion of our phantom. We decided to use polydimethylsiloxane (PDMS) for the solid portion of our phantom. PDMS is a silicon-based organic polymer often used in soft medical devices. PDMS is inert, non-toxic, and non-flammable, so it was an optimal material for the solid portion of our skin

phantom. Additionally, two pieces of PDMS can be bonded together easily, which allowed us to use a layered approach to our design. Carbon black is a carbon allotrope, usually sold in the form of a powder, which can be used as a dopant for polymers to change electrical properties. We used carbon black as a dopant for the bottom layer of our phantom, which gave our PDMS conductive properties.

Due to the novel approach that we adopted for our phantom design, we were unsure of how different factors would influence our measurements. As such, we decided to use simple salt solutions and phosphate-buffered saline as the liquids for our phantom. The exact concentration of these liquids will be explained in Chapter 7.

3.3 Fabrication

As shown in Figure 3.2, our phantom consists of three layers. Each layer is fabricated individually and assembled together into the completed phantom. All of the layers were fabricated in a clean environment to prevent contamination due to dust. This is especially important during assembly. An overview of our fabrication process is shown in Figure 3.3.

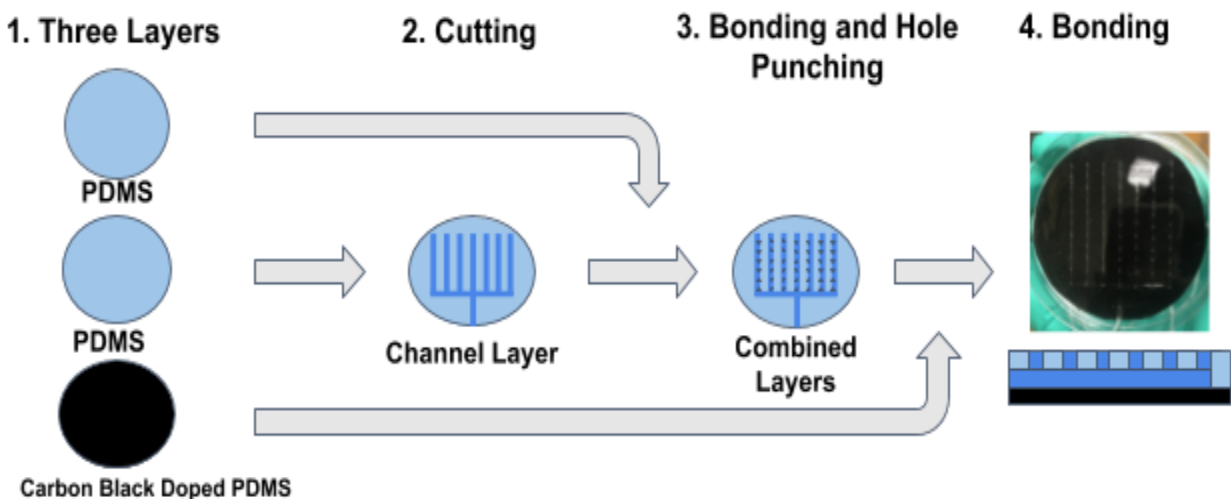


Figure 3.3: Overview of Fabrication Process

3.3.1 Flat PDMS Layers

Our fabrication process begins with the production of flat PDMS discs for each layer. The fabrication method for flat PDMS discs is as follows. We mixed 8 grams of PDMS (Dow Corning, Sylgard 184) in a 10:1 ratio of part a to part b for 15 minutes. After mixing, the PDMS was poured into a petri dish of dimensions 90 mm diameter and 15 mm height. The petri dish and PDMS were inserted into a vacuum desiccator for 30 minutes to remove any air bubbles trapped in the PDMS. Afterward, the PDMS was cured at 80°C for 2 hours on a level surface in an oven. After curing, the PDMS was removed from the petri dish, and a ring 1 mm from the edge of the resulting PDMS layer was cut to remove the uneven edge that formed on each layer. This ensures a PDMS layer of consistent thickness. Two of these layers are required for each skin phantom.

3.3.2 Carbon Black Doped Base Layer

Due to the much higher viscosity of PDMS with carbon black, a different procedure was needed to fabricate the carbon black PDMS layers. An overview of the process is outlined in Figure 3.4. Using the same method in section 3.3.1, we generated a PDMS layer using 5 grams of PDMS. Rectangular pieces with dimensions of approximately 4mm x 3mm were cut from the PDMS to be used as spacers.

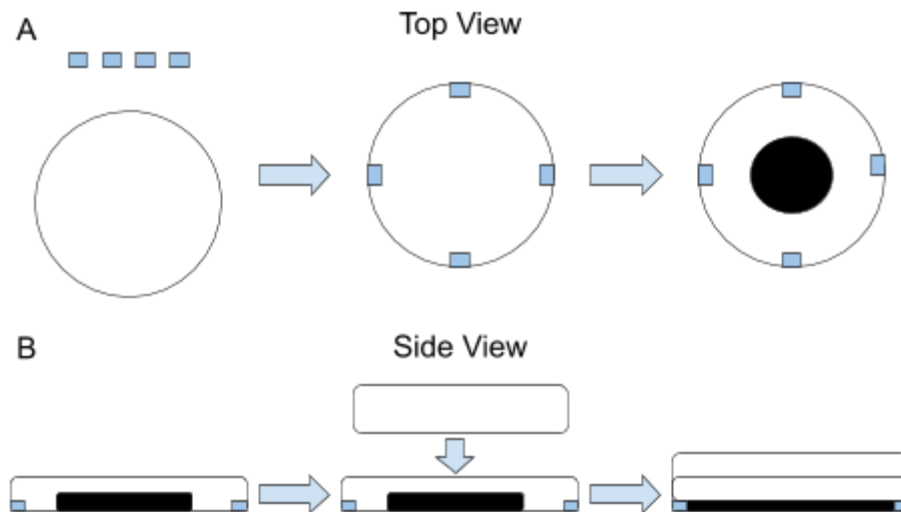


Figure 3.4: Carbon Black Layer Fabrication

We mixed 8 grams of part a with 2 grams of carbon black for 30 minutes. We then mixed part b into the mixture for 15 minutes. The mixture was then poured onto the underside of the lid of a petri dish along with the spacers as shown in Figure 3.4a. The carbon black PDMS was spread slightly manually until it resembled the final picture in Figure 3.4a, then the lid was placed in a desiccator for 30 minutes. The carbon black PDMS was flattened using the bottom of the petri dish as shown in Figure 3.4b and left alone for 1 hour. This step helps remove bubbles from the final layer. Afterward, the carbon black PDMS was cured and cut using the same method explained in the previous section.

3.3.3 Skin Phantom Cutting and Assembly

The middle layer of our phantom consists of liquid channels for our conductive solutions. We started by taking a flat PDMS layer from section 3.3.1. We cut trident shape channels shown in Figure 3.2 from a flat PDMS layer using Cricut Explore Air 2, a commercial cutting machine. After cutting, we carefully transferred the cut layer from the Cricut machine to a flat surface. We then treated the exposed portion of the layer and the second flat layer using air plasma as shown in Figure 3.5.

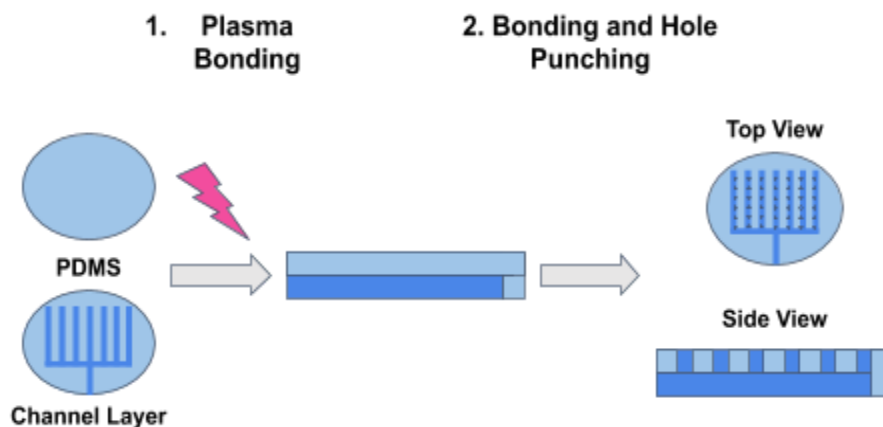


Figure 3.5: Bonding and Hole Punching Process

After bonding, we punch holes on the top layer using a syringe and a 20 ga dispensing needle. To complete the phantom, the carbon black layer is bonded to the middle layer using air plasma.

3.4 Syringe Pump

As mentioned previously, our skin phantom is designed to mimic the perspiration mechanism of the skin. Thus, a crucial part of our skin phantom is the fluidic system. A syringe pump was used to pump a conductive salt solution into the inlet of the phantom and out through pores. The syringe pump was connected to the skin phantom via Tygon tubing, as seen in Figure 3.6.

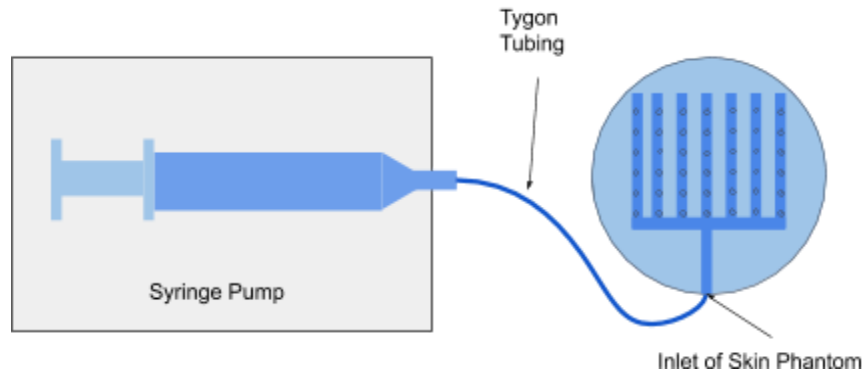


Figure 3.6: Syringe Pump Connected to the Inlet of Phantom Via Tygon Tubing

3.4.1 Flow Rate of Salt Solution

One parameter that needed to be set for our system was the flow rate of salt solution. As we are mimicking the perspiration mechanism of human skin, we decided to start with flow rates comparable to human perspiration rates on the abdomen. As mentioned in Chapter 1, average human torso perspiration rates are in the range of $1.2 - 11 \text{ g}\cdot\text{hr}^{-1}\text{m}^2$, which, when converted to units appropriate for the syringe pump, is $9.18 - 14.2 \text{ }\mu\text{g}/\text{min}$ [25,26].

4. Subsystem 2: Electrical Data Collection

4.1 Overview of Subsystem

The electrical data collection subsystem is used to collect and analyze the impedance vs. frequency data from our phantom. It consists of a Potentiostat, which utilized a five probe system, and the associated software, which collected the impedance vs. frequency data.

4.2 Potentiostat

A potentiostat is an instrument that keeps a constant voltage between the working and reference electrode by controlling the current going through the counter/auxiliary electrode. A simple schematic for a potentiostat is shown below in Figure 4.1 [28].

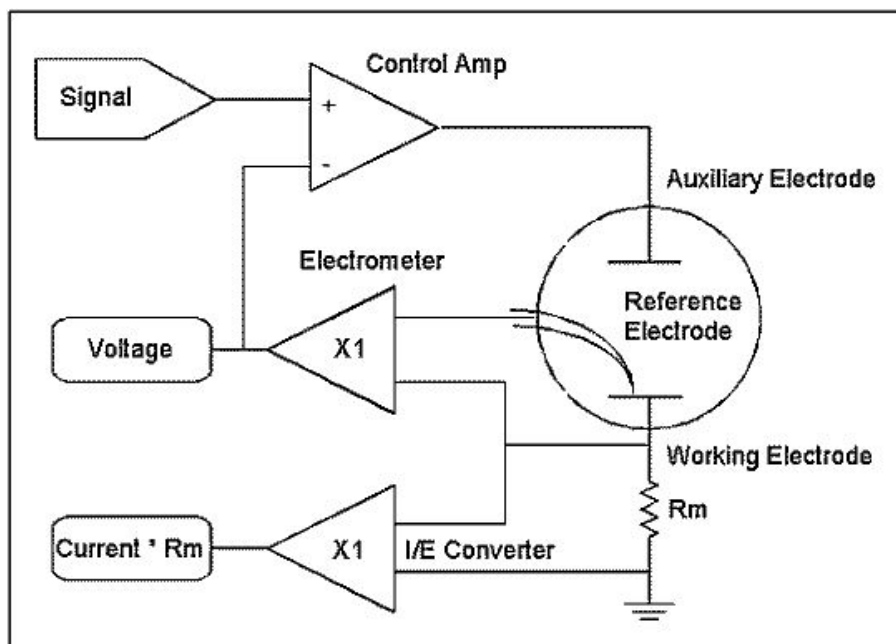


Figure 4.1: Potentiostat Schematic [28]

The potentiostat we used for our measurements was an Ivium Vertex with Electrochemical Impedance Spectroscopy (EIS) capabilities. This instrument was generously loaned to us by Jim Hutchison of Proteus Digital Health for the duration of our project. We needed a potentiostat

with EIS capabilities as we were interested in impedance vs. frequency behavior, and potentiostats without this function cannot perform frequency sweeps as we needed.

The Ivium Vertex also had galvanostatic capabilities, which means it could instead keep the current constant between the working and reference electrodes by altering the voltage using the counter electrode. We chose to use this setting as we wanted to ensure the current running through our phantom would always be at a safe level for humans. While we ensured no one touched the potentiostat during use, we wanted to make sure our phantom reflected accurate data at the same current levels you would use on a biowearable.

4.2.1 Probe System

The Ivium Potentiostat comes with four probes. Originally, we believed that the four probe system would be the best for our project. With four probes, current and voltage are supplied and connected to ground on their own separate connections and do not interfere with the other. When receiving the manual and block diagram for the potentiostat, we got the actual functions of each of the probes for the Ivium Potentiostat. From our contact at Proteus Digital Health, Jim Hutchinson, we were informed that the potentiostat would give us our desired results by connecting the working and counter probes for connection to one electrode and connecting the sense and reference probes for connection to the second electrode.

4.2.2 Software

The associated software for the Ivium Vertex potentiostat is IviumSoft. We used this software to set test conditions and to collect and export the impedance vs. frequency data. As mentioned previously, we chose to use the potentiostat's galvanostat capabilities and set the constant current level to be 1mA. This is a low enough level so that it is safe for human skin while being high enough that we can still get accurate readings with little noise interference. The specific test on the software we chose to use the "Impedance: Controlled I" test, which is a galvanostatic frequency scan at a fixed DC current.

While we are looking specifically at the 2,000 - 20,000 Hz range, we decided to run all tests from 10-100,000 Hz to get a better understanding of our phantom's impedance vs. frequency behavior. We chose to have 14 frequencies per decade, for a total of 57 frequencies tested. The input to the software is shown below in Figure 4.2.

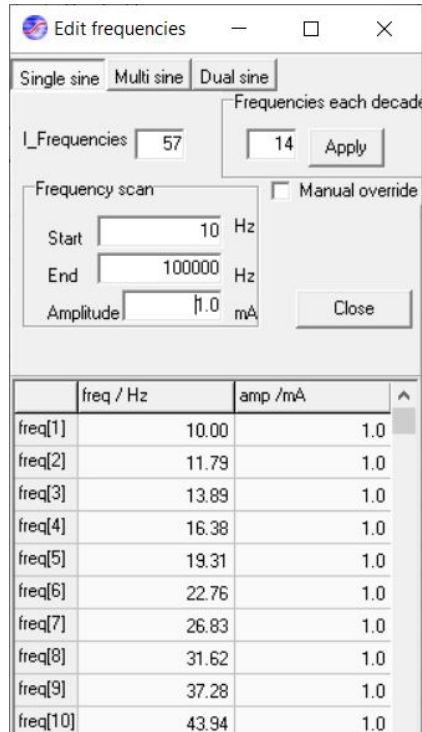


Figure 4.2: Test Conditions on IviumSoft

After running the test, the software would plot the magnitude (in Ohms vs. Hz) and the phase (in degrees). While this was a useful visual that aided us in ensuring our experimental set up was working properly, we chose to export the numerical data to Matlab for more in-depth analysis capability.

4.3 Initial Testing of Potentiostat

Prior to integrating the electrical measurement system with our physical model, we tested it on known quantities. First, we tested a 10 kOhm resistor. The resulting impedance vs. frequency plot is shown below in Figure 4.3, against the expected impedance vs. frequency plot.

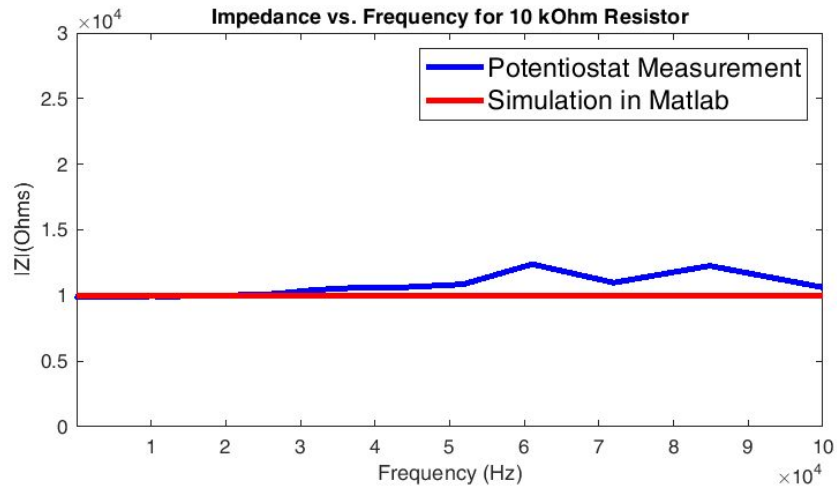


Figure 4.3: Impedance vs. Frequency for 10kOhm resistor

The impedance of a resistor should remain constant with changes in frequency. The values from the potentiostat are as expected for the most part; there are irregularities after 30,000 Hz.

However, we are most concerned with the 2,000-20,000 Hz range, so this should not affect our testing.

5. Subsystem 3: Circuit Model for Skin

5.1 Overview of Subsystem

The purpose of the circuit model for skin is to simulate skin's capacitive and non-linear behavior, which can be modeled by a memristor in parallel to a capacitor. To simulate a memristor, we used a program called Advanced Design Systems, ADS, which is an electronic design automation software system developed by Keysight.

5.2 Data Provided by Proteus Digital Health

Jim Hutchison of Proteus Digital Health generously gave us the analytics depicted in Figure 5.1. This plot, which he gathered by collecting data from his own skin, is on a linear scale. From the plot we can see that the actual values change from individual to individual. Thus, we decided our skin phantom should match the impedance vs. frequency *behavior* of skin, not the actual values. Specifically, our skin phantom aims to mimic the skin's capacitive and non-linear behavior. For our analysis, we will use Jim Hutchison's data as the benchmark, as it was obtained using the same potentiostat we used to collect data.

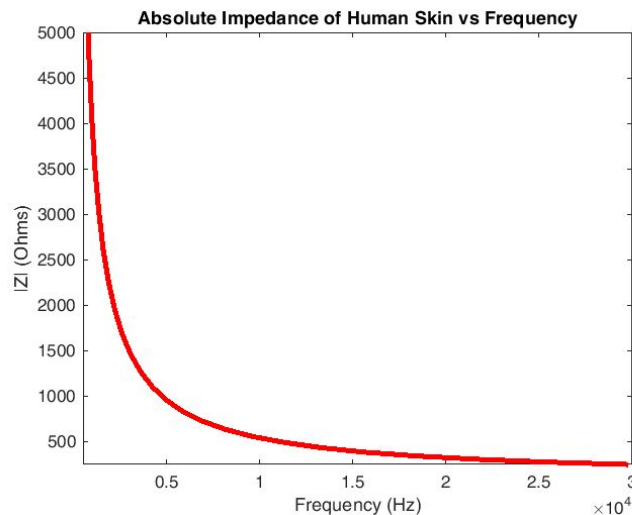


Figure 5.1: In-Vivo Skin Impedance vs. Frequency Data from Proteus Digital Health

5.3 Early Circuit Model for Skin

The circuit shown in Figure 5.2 is the first electric circuit model for skin published in 1998. The design includes R_s , which represents the resistance of the deep tissue of skin, in series with the parallel placement of C_p and R_p , which models skin's impedance. Finally, C_{pol} and R_{pol} , meaning a polarized capacitor and resistor, in series model an electrode.

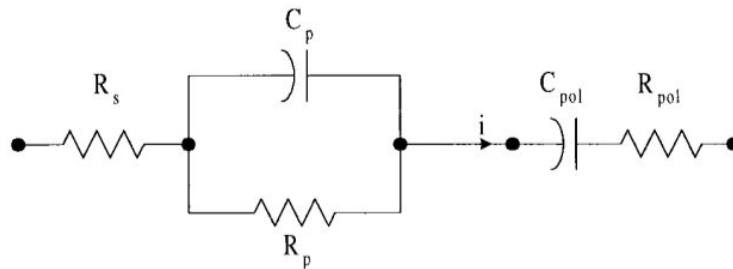


Figure 5.2: First Circuit Model for Skin

Proteus Digital Health gave us a circuit similar to this circuit model for skin, shown in Figure 5.3. Using the potentiostat, we obtained impedance vs. frequency data for this circuit and compared it to the data obtained from a simulation in Matlab, as seen in Figure 5.4.

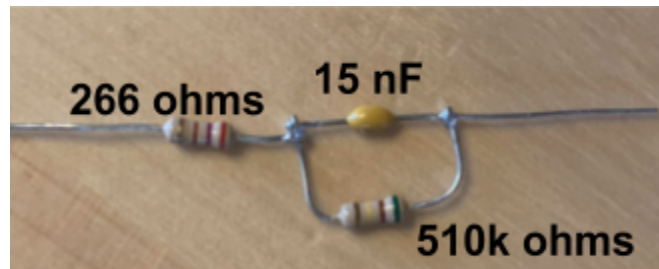


Figure 5.3: Simple Skin Equivalent Circuit Model from Proteus Digital Health

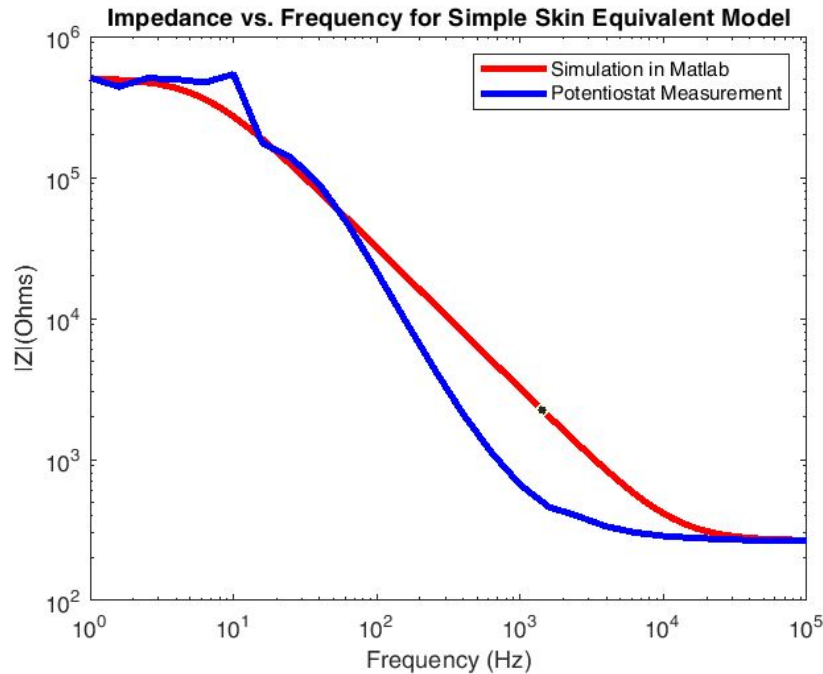


Figure 5.4: Impedance vs. Frequency for Simple Skin Equivalent Model

5.4 Updated Circuit Model

An updated 2018 paper models the electrical circuit of skin, shown by Figure 5.5, with a sweat duct memristor in parallel with a capacitor, which characterizes the capacitive properties of the stratum corneum, in parallel with a memductor, which represents skin's ability to conduct current.

An electrical measurement is considered non-linear when the applied stimulus itself affects the electrical properties of the underlying tissue. The skin exhibits such non-linear properties under voltage stimulus due to its sweat ducts and surrounding tissue, such as its upper layer – the stratum corneum.

For example, if you apply a constant, low-frequency sinusoidal voltage of high amplitude to human skin, the shape of the current differs from the sinusoidal pattern. This observation implies that the measurement is non-linear, and electro-osmosis, the directed motion of liquid caused by an electric field, within the sweat ducts is believed to be the underlying cause. So we can use a

memristor to model skin because voltage-current plots of non-linear systems exhibit hysteresis loops, which is the fingerprint of the memristor.

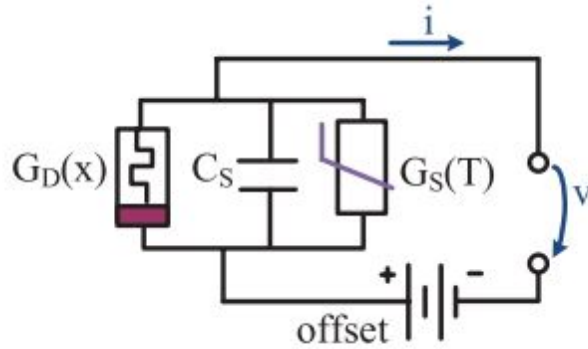


Figure 5.5: Updated Circuit Model for Skin

5.5 Skin & Memristor Properties

Table 5.1 below shows how skin's properties, which relate to memristor properties, are reflected in the I-V curve of a memristor. Skin's response to a dynamic load reflects a memristor's behavior to switch between on and off states, which forms the hysteresis loop seen in its I-V graph. Skin's sweat ducts relate to an important state variable of the memristor – the galvanic contact – which is the amount of ionic charges passing through the skin. The equation to the right depicts this system. The non-linear behavior of skin connects to the non-volatility of a memristor, giving it the ability to remember past signals flowing through it. Lastly, the skin's ability to alter ionic movement correlates to memristors' behavior towards frequency, where its hysteresis loop flattens as frequency increases.

Skin's Property	Memristor Property	Memristor I-V Curve
Skin's response to dynamic load	Dynamic Response	Forms hysteresis loop
Sweat ducts	Galvanic Contact	$M(t) = R_{ON}(x(t)) + R_{OFF}(1 - x(t))$
Non-linear behavior	Non-volatility	Resistor with memory
Alters ionic movement	Frequency	Flattens hysteresis loop

Table 5.1: Skin & Memristor Properties

5.6 ADS Model & Simulation

The electrical circuit for a memristor constructed in ADS is depicted in Figure 5.6. The first op-amp acts as a summing amplifier, which adds the input voltage and the output of the voltage multiplier, V_Z . The second op-amp, along with R4 and C1, acts as an integrator. The frequency band of operation, which is up to 16 kHz, is determined by R4 and C1. Lastly, you see the outputs of the summing and integrating op-amps being fed into the voltage multiplier to produce V_Z . Figures 5.7, 5.8, and 5.9 display the voltage node equations for V_{SUM} , V_{INT} , and V_Z .

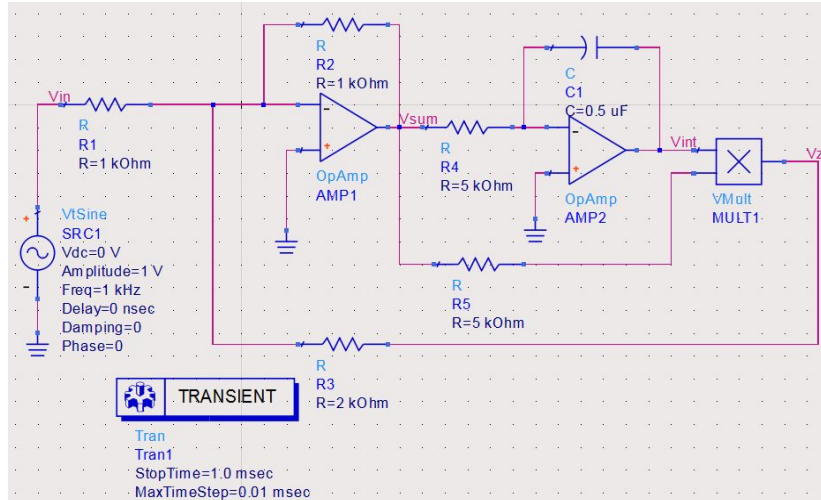


Figure 5.6: ADS Memristor Circuit

$$V_{sum} = \left(-\frac{R2}{R1}\right) \cdot V_{in} + \left(-\frac{R2}{R3}\right) V_z$$

Figure 5.7: V_{SUM} Node Equation

$$V_{int} = \left(\frac{-1}{R4 \times C1}\right) \int V_{sum} dt$$

Figure 5.8: V_{INT} Node Equation

$$V_z = V_{sum} V_{int} = \left(\frac{-1}{R4 \cdot C1}\right) \int V_{sum}^2 dt$$

Figure 5.9: V_z Node Equation

And Figure 5.10 shows the hysteresis loop generated by the previous memristor circuit, which models the non-linear behavior we've replicated with our skin phantom.

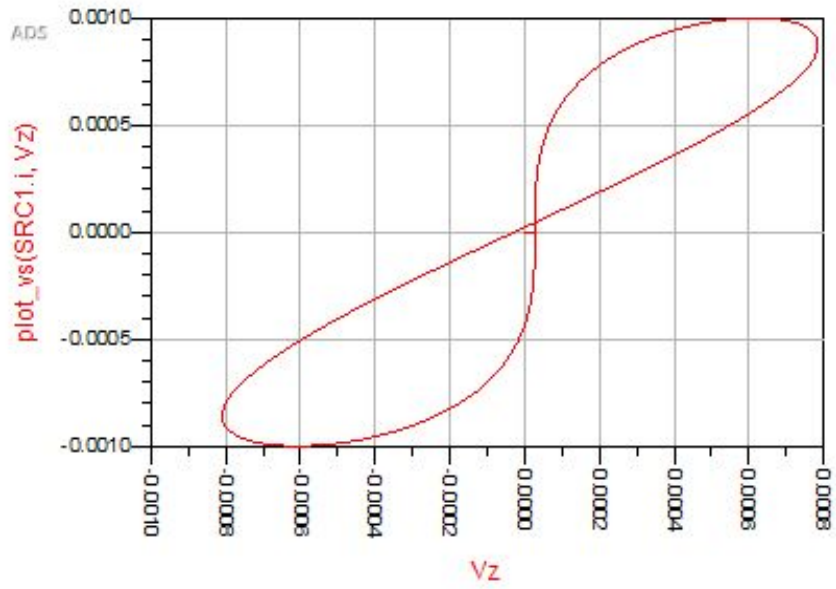


Figure 5.10: Memristor Hysteresis Loop

6. Computer Simulations of the Skin Phantom

6.1 Overview of the Subsystem

This subsystem was all completed on Computer Simulation Technology Studio Suite® simulation software, which will now further be referred to as CST. CST is a high-performance 3D Electromagnetic analysis software.

The original purpose of the CST simulation of our phantom was to do factor variation of our phantom and determine which factors actually influenced the data and closely produced the results that we expected to see. We were planning on testing different materials, different geometries, as well as the various factors we chose to implement in our physical experiments. It was also desired that the CST simulations showed an irrefutable correlation and confirmation of our physical experiment. However, there was a steep learning curve for the software. The software is typically used to analyze the performance and efficiency of antennas and filters, electromagnetic compatibility and interference (EMC/EMI), exposure of the human body to EM fields, electro-mechanical effects in motors and generators, and thermal effects in high-power devices [29]. While it could produce the impedance vs. frequency graph we needed it to produce, there were no previous projects we found in our discovery phase that could mimic a potentiostat measuring a certain material. Shown in the next subsections, we did a baseline simulation to determine which exciting port would be the best to continue our experiments.

For the purpose of our project, S-Parameters, or Scattering Parameters, were evaluated, which describes the input-output relationships between ports in an electrical system. The software, in addition to the S-Parameter graphs, was also able to produce the Z-matrix graph, which gives us our desired plot of impedance vs frequency. Since impedance for skin is a combination of resistance and capacitance, CST also made it possible to view the characteristics of those individually by producing capacitance and resistance graphs. In our simulations, we used both waveguide ports and discrete ports in our simulations. A waveguide port simulates an infinitely long waveguide connected to the structure, enabling the stimulation as well as the absorption of energy. A discrete port consisting of a current source with an inner impedance that excites and

absorbs power, connected to two flat sheets of PEC on the top and bottom.

6.2 Baseline - “Hello World” Test

To confirm that the software was producing the correct data for the material being evaluated in the software, we did a baseline test, our CST version of a “Hello World” test, to confirm the results of the software. We decided to make a capacitor, using two waveguide ports and silicon dioxide as the dielectric as shown in figure 6.1. Making a capacitor with known material properties ensured that we were able to calculate and confirm the results produced by CST. The red surface with the ‘2’ is the negatively charged waveguide port, and the positively charged waveguide port is not shown in the photo but is on the bottom side of the cube. The blue-green cube between the silicon dioxide.

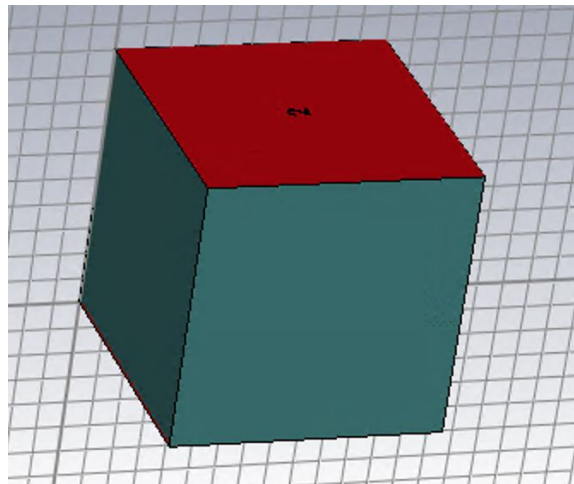


Figure 6.1: Silicon Dioxide Capacitor Simulation

To ensure that we were seeing the correct capacitance shown in Figure 6.2 We calculated the capacitance by using the formula:

$$C = \frac{\epsilon A}{D} \quad \text{equation 6.1}$$
$$C = \frac{3.7 \times (8.85 \times 10^{-12}) \times (1 \times 10^{-6}) m^2}{(1 \times 10^{-3}) m}$$
$$C = 3.256 \times 10^{-14}$$

This calculation confirmed the results shown in Figure 6.2. The graph is the capacitance of the capacitor.

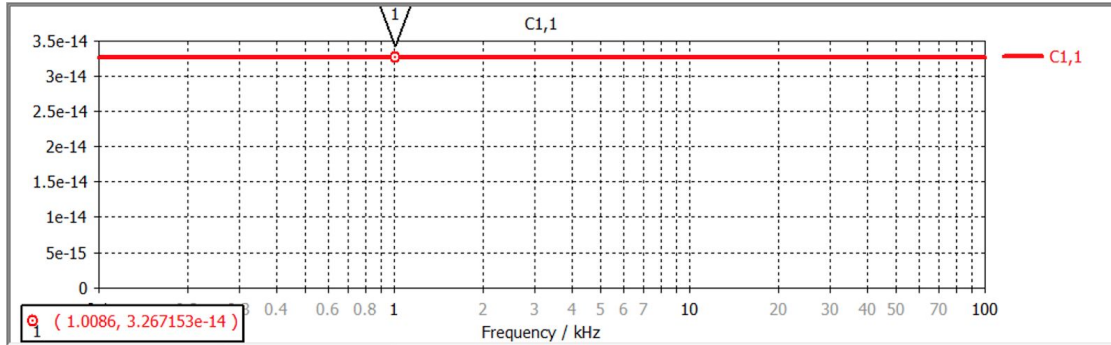


Figure 6.2: Capacitance of Silicon Capacitor

Next, we looked at the Z-Matrix or impedance vs frequency graph produced when making the silicon dioxide capacitor. We noticed that when put into a log scale, it produced a linear line that reflected the correct values for the equation:

$$\text{Impedance: } \frac{1}{j\omega c} \quad \text{equation 6.2}$$

To prove this, we used decades 1kHz and 10 kHz to see if the values were accurate:

$$\text{Impedance at 1 kHz: } \frac{1}{j(2\pi 1,000)3.25 \times 10^{-14}}$$

$$\text{Impedance at 1 kHz: } 4.882 \times 10^9$$

and

$$\text{Impedance at 10 kHz: } \frac{1}{j(2\pi 10,000)3.25 \times 10^{-14}}$$

$$\text{Impedance at 10 kHz: } 4.882 \times 10^8$$

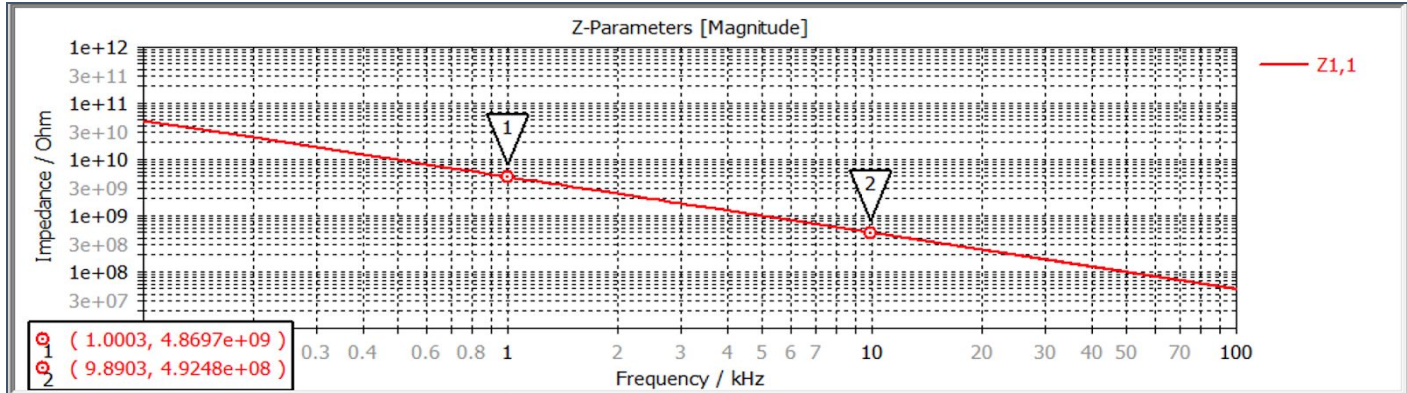


Figure 6.3 : Graph of $\frac{1}{j\omega c}$

6.3 Material Simulations

CST has an extensive material library in which each material is preloaded with the respective properties. The properties that are important are shown in a material property box. The figures shown in the box mean the following: Type: Can be defined as normal, PEC, or lossy metal. Epsilon/Dispersive Epsilon: This is the permittivity. Permittivity plays an important role in determining the capacitance of a capacitor. The Nth order model means the inputs of epsilon changing over frequency were not given for the frequency range under evaluation, and the program has to extrapolate for the values. Mu is a measure of the amount of resistance encountered when forming a magnetic field in a classical vacuum. Electrical Conductivity simply means the electrical current a material can carry or its ability to carry a current. Rho is the density.

6.3.1 CST Skin

To simulate the impedance vs freq behavior of skin, we used CST's Bio Tissue: Skin material for this simulation. The material properties for this biomaterial are shown in Table 6.1.

Material	Type	Epsilon/Dispersive Epsilon	Mu	Rho (kg/m ³)	Electric Conductivity (S/A)
Bio Tissue/Skin	Normal	Nth order, N=3	1	1100	N/A
Carbon_Black+ PDMS	Normal	7.7	1	2000	0.045
PDMS	Normal	2.5	1	N/A	2.5x10 ⁻¹⁵

Table 6.1: Material Properties of Materials used in CST Simulations

We made a 1mmx1mm cube and placed two oppositely excited waveguide ports on the top and the bottom. This is shown in Figure 6.4. The graph produced by the simulation, shown in Figure 6.5, shows that skin actually does produce the trend we expect to see. For these simulations, we are looking for the trend and ignoring the magnitude, since the sizes of the simulated material are not the same as in real life.

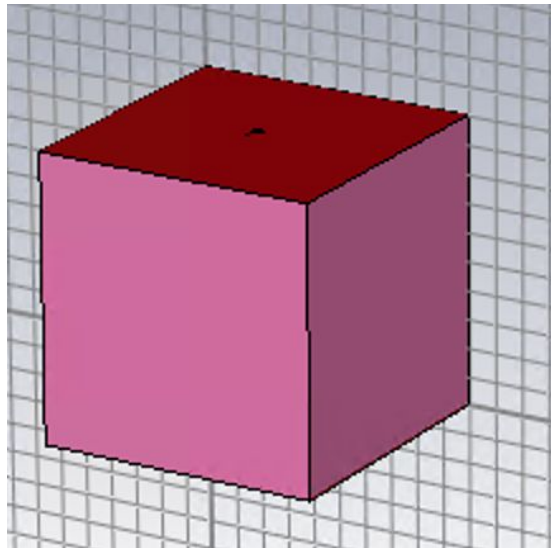


Figure 6.4: Bio/Tissue Skin 1mmx1mm Cube

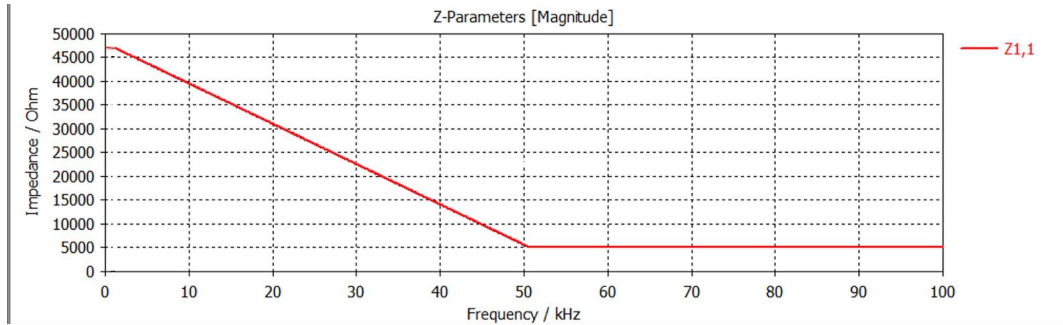


Figure 6.5: Impedance Vs. Frequency of Bio/Tissue Skin

6.3.2 Simplified Model of Skin - Wet Vs. Dry

Next, we made simplified skin models of three layers: Skin, Fat, and Muscle. The main difference between the models is the top layers: one being dry skin, the other being wet skin. Figure 6.6 is the model with dry skin and Figure 6.8 is the model with wet skin. The purpose was to confirm that the presence of liquid would produce a more conductive model that would more closely match the expected trend of impedance vs frequency for the skin.

We had to make the materials in CST because dry skin, wet skin, muscle, and fat were not in the database. To this, we used the website “Calculation of the Dielectric Properties of Body Tissues - in the frequency range 10 Hz-100 GHz” by the Italian National Research Council. The important material properties for the purpose of the simulations were epsilon and tangent delta. In 10 Hz increments, from 10 Hz to 100 kHz, the website gave the values for each of those variables. We then imported them into an excel sheet and uploaded the values into CST for each material.

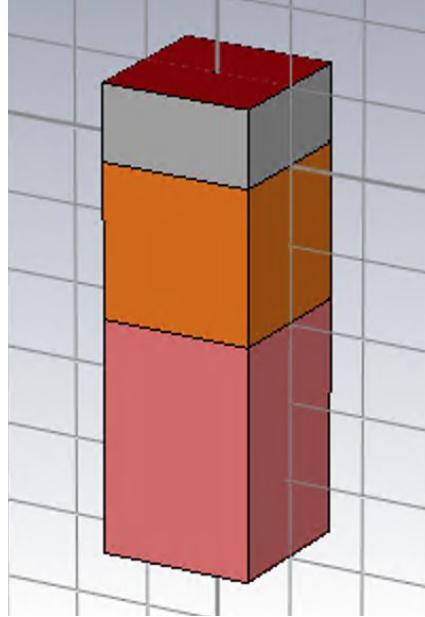


Figure 6.6: Dry Skin 1mmx1mm, Fat 1mmx3mm, Muscle 1mmx5mm

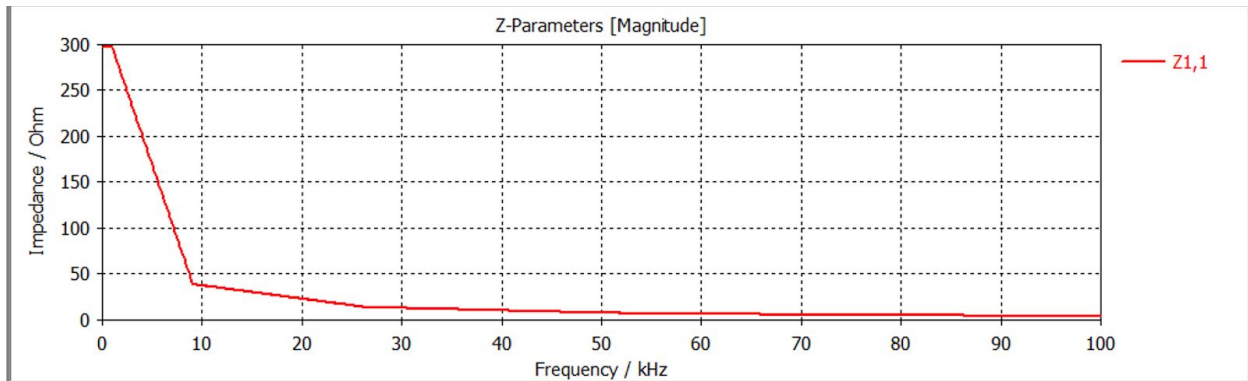


Figure 6.7: Impedance Vs. Frequency of Simplified Skin Model - Dry

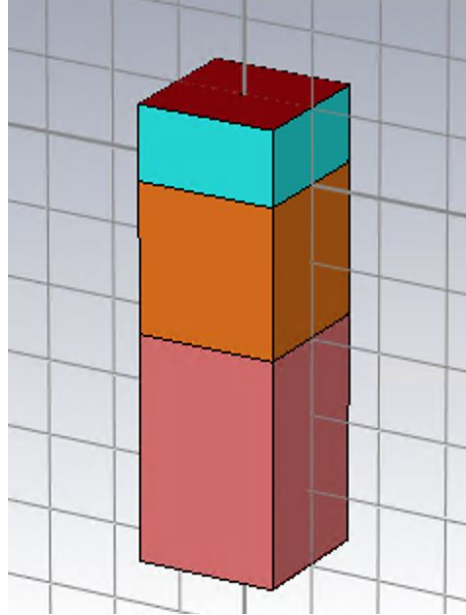


Figure 6.8: Wet Skin 1mmx1mm, Fat 1mmx3mm, Muscle 1mmx5mm

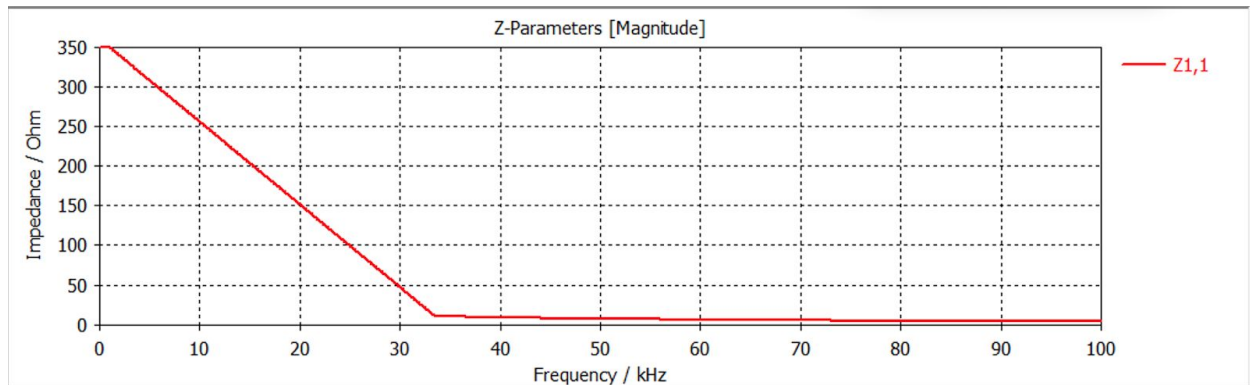


Figure 6.9: Impedance Vs. Frequency of Simplified Skin Model - Wet

When comparing Figure 6.7 and 6.9, it is clear that the slope associated with the wet skin is more closely shaped to our expected impedance vs. frequency of skin. Verifying that wet skin is a better conductor did multiple things for the development of our skin phantom. It confirmed that the saline or PBS solution we were going to use for our phantom was going to make it perform more accurately in terms of the electrical properties of the skin. It also confirmed that a good variable to change in our physical experiments was the content of the water solution and the flow

rate (mimicking our perspiration levels).

6.3.3 Carbon Black + PDMS

The next step was to simulate the individual materials of the phantom. The purpose was to confirm that our chosen materials were functioning how we thought they would. Skin acts as a low pass filter. Since the design for the phantom is to have the phantom conductive throughout by having the carbon black + PDMS layer on the bottom with conductive liquid connecting the top two PDMS layers, it is assumed that the carbon black would act as a resistor due to its conductivity.

Carbon black mixed into PDMS is not a unique application, however, the way we created the layer was unique for each sample. The conditions and material measurements were the same samples, however, the samples were hand-mixed, so there was no guarantee that the PDMS was exactly equally distributed throughout the PDMS. This means that there was a possibility that our actual carbon black + PDMS sample could have a slight capacitive effect and lower electrical conductivity because of slight gaps and unequal distribution between the carbon black particles in the PDMS. After research, we determined that there were no electrical properties of carbon black mixed into PDMS documented. In the Santa Clara University Lab, we were going to use the N1501A Dielectric Probe Kit to find our samples' exact dielectric properties. This would have made the simulations the most accurate. However, due to COVID-19, this plan had to be revised because we were not allowed in the labs for testing. In order to get the property values we needed, we used an educated guess of what the epsilon and electric conductivity would be from academic papers that found these properties of carbon black in other purposes and in other mixtures. The material properties are shown in Table 1. It should be noted that while carbon black is an extremely conductive material, it is mixed into a highly non-conductive material, so the electrical conductivity of our sample is expected to be much lower but still actively conductive.

For the simulation of the carbon black sample, we switched to circular cylinders to more accurately mimic the shape of our Skin Phantom. For the simulation excitation, after a lot of experimentation, we found that the waveguide ports worked best with squares. We then switched to a discrete port. As explained above, a discrete port consists of a current source with an inner impedance that excites and absorbs power, connected to two flat sheets of PEC on the top and bottom. The requirement of the discrete port is that it has to be connected (on both the top and bottom) with conductive metals. We chose PEC to simplify our simulations and ensure that the electrode was not affecting the results. Figure 6.10 shows the carbon black + PDMS simulation setup.

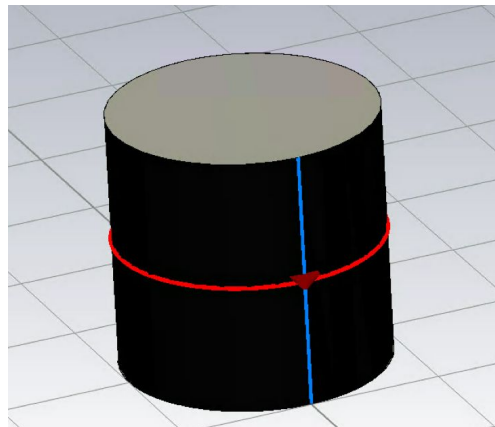


Figure 6.10: Carbon Black + PDMS Sample With Discrete Port and PEC sheets

The results are what we expected. The Carbon Black, theoretically, should act as a resistor with high impedance, as shown in Figure 6.11. There was a slight discrepancy with our real sample, but we determined that is from the hand mixing process that could have resulted in the carbon black particles not being evenly distributed in the PDMS.

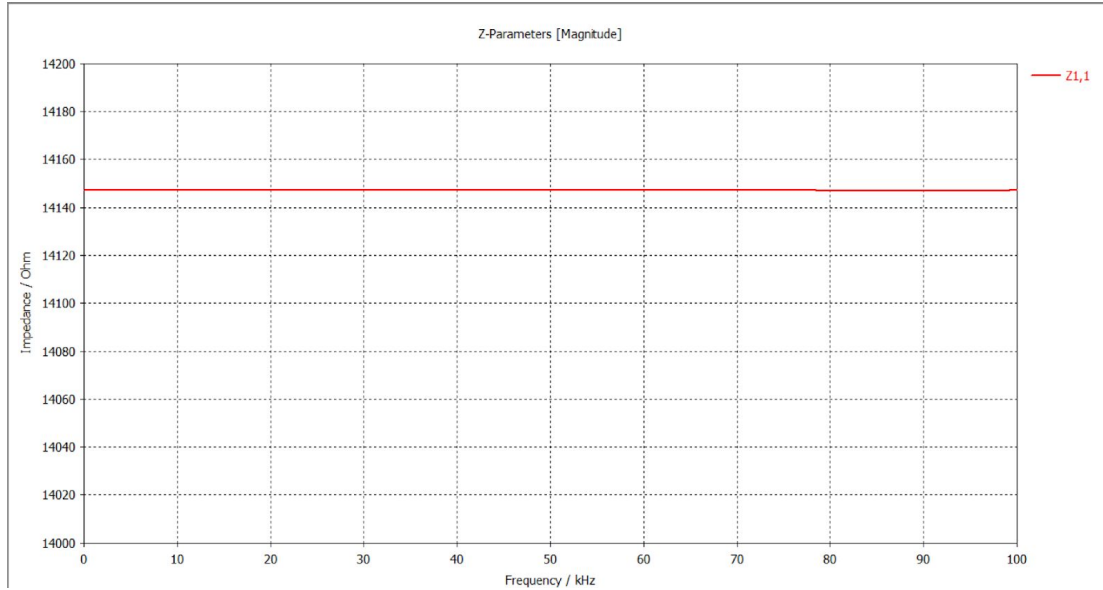


Figure 6.11: Impedance VS. Frequency Graph of Carbon Black + PDMS

6.3.4 PDMS

We assumed that PDMS was going to act like a capacitor because of its extremely low electrical conductivity. Unlike carbon black, we were able to find the electrical properties of PDMS online and was successfully able to simulate with accurate values. Table 1 shows the PDMS simulation set up.

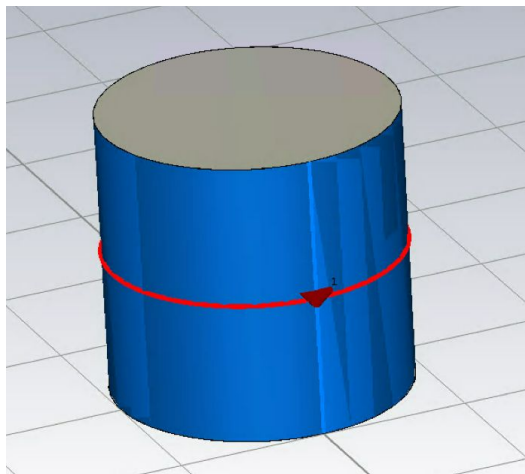


Figure 6.12: PDMS Sample With Discrete Port and PEC sheets

The results are what we expected. PDMS, theoretically, should act as a capacitor that changes impedance value over a change of frequency, as shown in Figure 6.13. The impedance value was incredibly high, which matched our actual measurements of the PDMS sample.

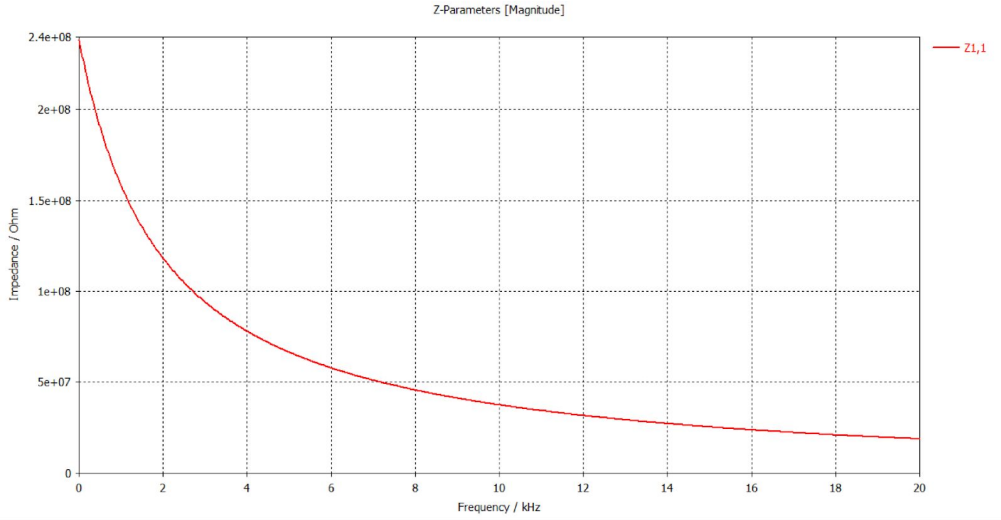


Figure 6.13: Impedance VS. Frequency Graph of PDMS

6.3.5 Simplified Model of Skin Phantom

Lastly, due to difficulty in the simulation of the model of the actual skin phantom design in CST, we made a simplified model to show the effect of the materials when stacked on each other, shown in Figure 6.14.

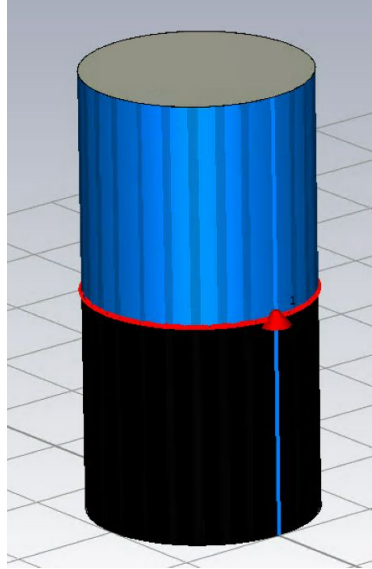


Figure 6.14: Simplified Model of PDMS on Top of Carbon Black

The graph shown in Figure 6.15 shows what we expected. This graph, instead of showing simply the Impedance vs. Frequency of the materials, show the real and imaginary components of the simplified phantom. It has a very high resistance value (the real value), and has a slight capacitive effect (the imaginary value).

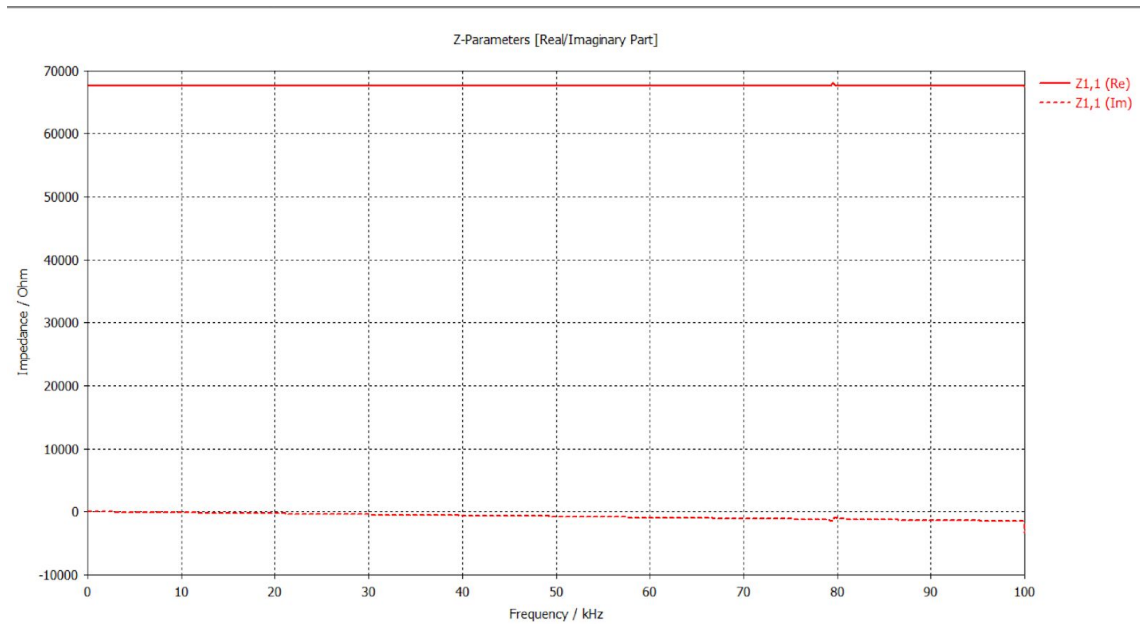


Figure 6.15: Real and Imaginary Components of the Impedance Vs. Frequency of Simplified Circuit

6.4 Future Work

The next team will be picking up and doing the following with CST: because of the complex geometry, as shown in Figure 6.16. The way we were simulating with both waveguide ports and a discrete port was taking a very long time and often wouldn't complete the calculations. They will be determining how to correctly simulate a complex geometry such as this. They also will be able to test other materials and do factor variation through simulation.

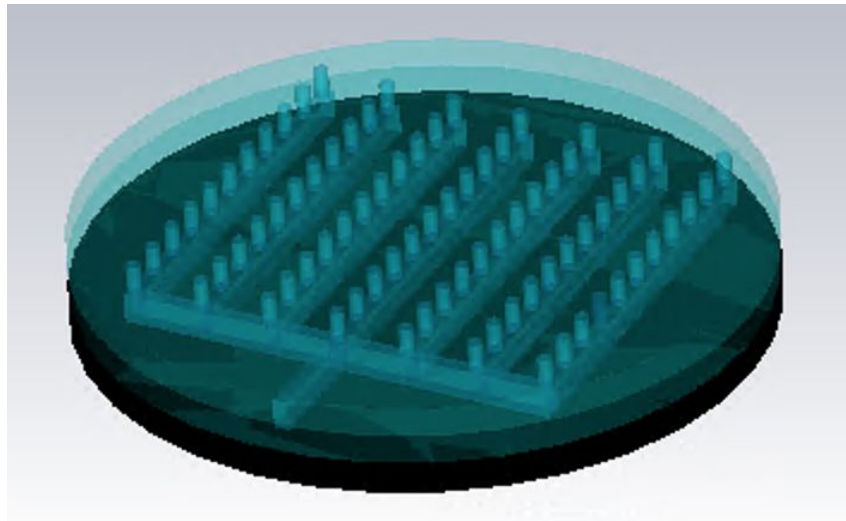


Figure 6.16: CST Model of Actual Skin Phantom

7. System Integration, Testing, and Analysis

7.1 Integrating the Physical Model and Electrical Measurement System

The physical model and the electrical measurement system were integrated as seen below in Figure 3.1. To establish electrical contact between the potentiostat and the physical model, we used stainless steel probes connected to steel shim electrodes. Electrodes were placed on the top and bottom of the physical model, and a weight was placed on top to ensure good contact.

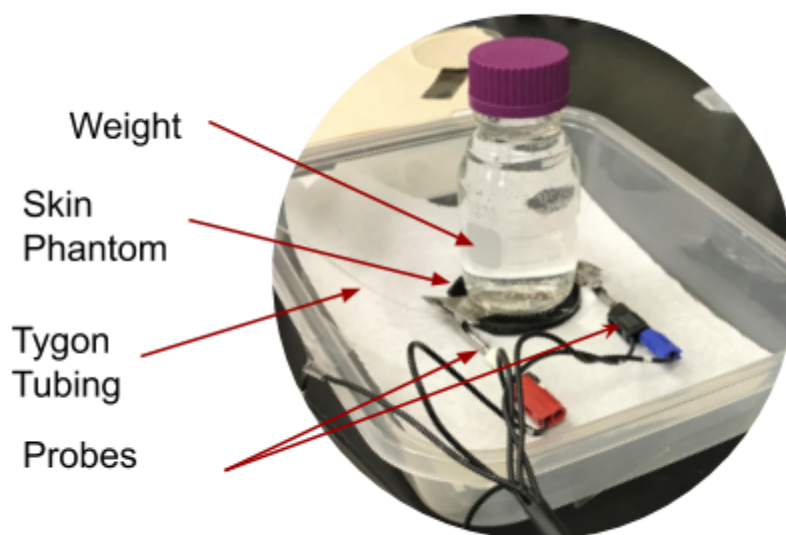


Figure 7.1: Integration of Physical Model and Electrical Measurement System

7.1.1 Preliminary Results

Initial tests were performed only on the base carbon black doped PDMS layer. Our initial layer was approximately 3mm thick; as seen below in Figure 7.2, the impedance vs. frequency curve for this thick carbon black layer was inconsistent, highly irregular, and not a good match for human skin. This was likely because the layer was too thick and not conductive enough for the electrical signal to pass through. To test this hypothesis, we created a carbon black doped layer with 1.5 mm thickness. The resulting impedance vs. frequency curve for that thin carbon black layer is also plotted below in Figure 7.2.

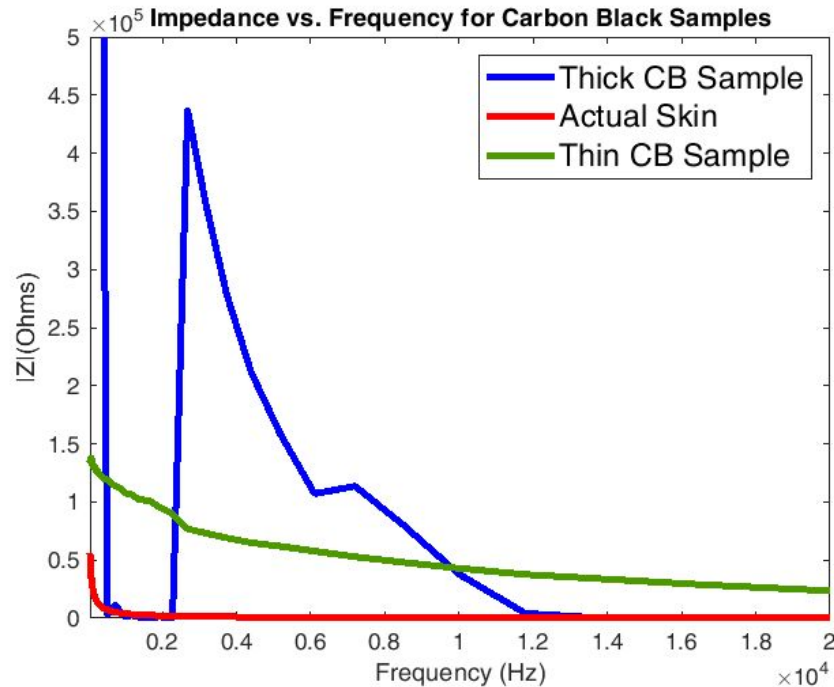


Figure 7.2: Impedance vs. Frequency for Thick and Thin Carbon Black Layers and Skin

The thin carbon black layer resulted in an impedance vs. frequency curve that was more uniform and gave behavior similar to what we were expecting: a capacitor in parallel with a resistor. The thin carbon black layer was a better match for the skin's impedance vs. frequency behavior; thus we decided to change our base carbon black layer to a thickness of 1.5 mm. As we mentioned previously, skin impedance vs. frequency behaves similarly to a resistor in series with a resistor and capacitor in parallel. The carbon black matches the behavior of the second part of that simplified circuit; the remaining resistance will be mimicked by the salt solution.

Another preliminary test we performed was testing the impedance vs. frequency for several different salt solutions: 40 mmol NaCl, 65 mmol NaCl, 154 mmol NaCl, and 1x Phosphate Buffered Saline. We placed 30 mL of solution in a plastic petri dish, then stuck the stainless steel alligator clip probes in the petri dish, on opposite sides. We were expecting the salt solutions to have impedance vs. frequency curves similar to a resistor; that is, constant with respect to frequency. The impedance vs. frequency curves of those liquids are shown below in Figure 7.3.

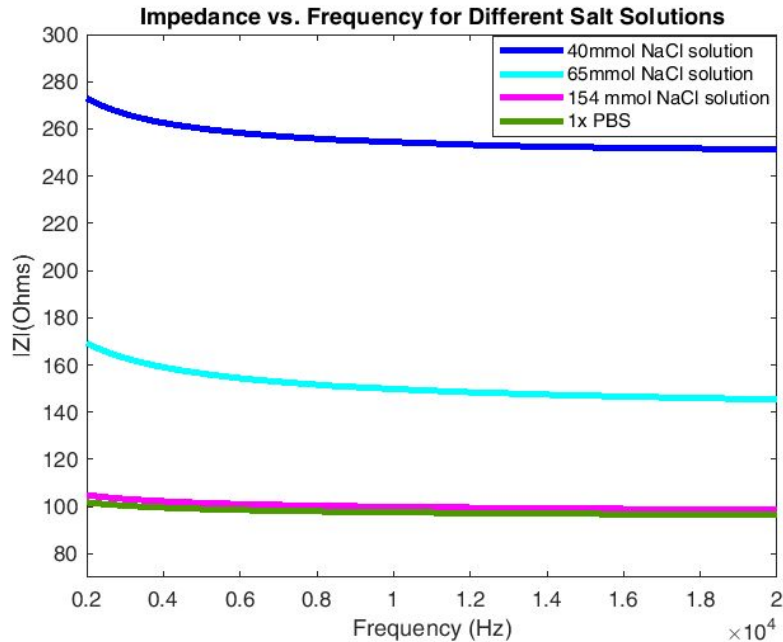


Figure 7.3: Impedance vs. Frequency for Different Salt Solutions

Figure 7.3 shows that the impedance vs. frequency behavior for the different salt solutions does not change significantly, only the magnitude differs greatly. As we are exclusively looking at the impedance vs. shape behavior, magnitude is not a significant consideration for the choice of salt solution. Thus, we chose to work with 154 mmol NaCl and 1x PBS as they are slightly closer to the behavior of a resistor, as we expected.

7.2 Full Factorial Experiment

As our phantom was designed to be easily customizable, a full factorial experiment was designed to analyze the effects of different variable factors on our skin phantom's impedance vs. frequency behavior. A full factorial experiment is one where every possible combination of factor levels are tested in order to understand their individual and combined effects on our phantom's impedance vs. frequency behavior.

Four factors that we predicted would make a difference to our phantom's behavior were pore density, salt solution concentration, flow rate, and the presence of a membrane. We predicted that increasing pore density, salt solution concentration, and flow rate would decrease the

phantom's resistance, while the addition of a membrane would increase the phantom's capacitance. We chose high and low levels for each factor, as shown in Figure 7.4. The pore densities were chosen based on what we could feasibly fit into the phantom. Salt solution concentrations were based on the aforementioned preliminary test of different salt concentrations. Flow rates were based on the average human torso perspiration rate. A wax paper membrane was chosen due to its impermeability causing it to act as a dielectric.

Factor	High Level	Low Level
Pore Density	1 pore / 3 mm	1 pore / 5 mm
Salt Solution	NaCl Stock solution (154 mmol NaCl)	1x PBS (137 mmol NaCl)
Flow Rate	14.2 μg / min	9.18 μg / min
Membrane	Nonpermeable wax paper membrane	No membrane

Figure 7.4: Levels for Each Factor in Full Factorial Experiment

Four factors with two levels each necessitated sixteen tests for a full factorial design. We ran two replicates for a total of thirty-two datasets. We ran tests in random order to ensure statistical validity. Additionally, we flushed the phantom out with DI water in between tests to ensure there was no salt build-up within the channels. This experiment was performed over the course of one afternoon to ensure little variation in external testing conditions. As our phantom is easily customizable, we were able to change salt solutions, flow rates, and membranes on the same phantom. Pores are punched directly into the top PDMS layer, so pore density is not changeable on a phantom once it is made. Thus, we used two phantoms, one with high pore density and one with low pore density, for this experiment.

7.2.1 Experimental Procedure

We randomized the two sets of sixteen tests prior to the experiment and referred to this order while setting up each test. First, we would check to see which pore density was being tested, high

or low. This would determine which phantom we would be using. We would then flush out that phantom with DI water to ensure there was no residual salt in the channels.

Next, we would check to see which salt solution we were testing, the higher concentration (our NaCl salt solution), or the lower concentration (1xPBS). We would then prefill the phantom with the appropriate solution using a Luer lock syringe, dispensing tip, and Tygon tubing connected to the inlet of the phantom. We ensured all channels were filled with the solution, but none was coming through the pores. The phantom was then set in a plastic tub to catch any spillage during the experiment.

Third, we would check which flow rate the test called for, high or low. We would set the appropriate flow rate on the syringe pump.

Finally, we would see whether or not the test called for a wax paper membrane. If so, we would place it on the top of the phantom. Then, we would place electrodes on the top and bottom of the phantom and clipped on the probes leading to the potentiostat. To ensure proper and consistent electrical contact, we would place a weight on top of the upper electrode. Finally, we would start the syringe pump, and wait thirty seconds to allow flow to begin. Using the associated software (explained previously in Chapter 4), we would then run the impedance vs. frequency sweep, ensuring that no one was touching any part of the test setup. After the test was finished, we would save the collected data and move on to the next test, following the order set prior to the experiment.

7.2.2 Experimental Results

As mentioned previously, our experiment resulted in thirty-two impedance vs. frequency datasets or our skin phantom, with 2 datasets for each test condition. Those thirty-two datasets are plotted below in Figure 7.5 against our *in-vivo* skin benchmark data.

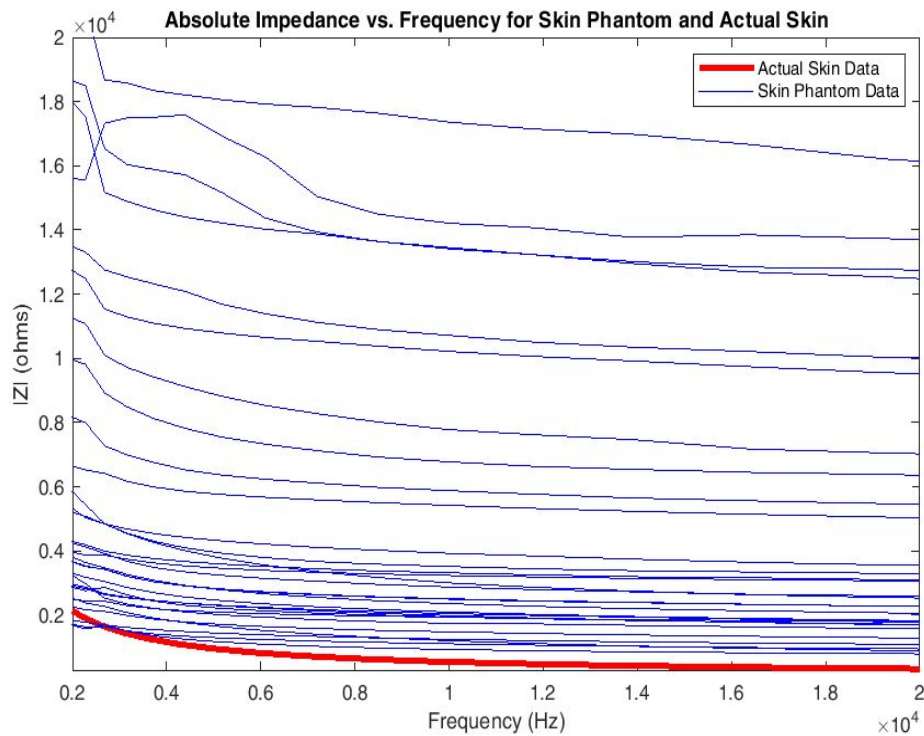


Figure 7.5: Impedance vs. Frequency for *In-Vivo* Skin and 32 Skin Phantom Datasets

In order to more closely understand the impedance vs. frequency behavior of skin, and how our phantom’s data compared, there is a zoomed-in plot of our experimental data shown in Figure 7.6. Note that no datasets were discarded as outliers from analysis despite not being shown in Figure 7.6; this plot was simply to demonstrate the behavior trends more clearly. All thirty-two datasets were used in our analysis of results. Figure 7.6 demonstrates that our skin phantom has several test cases that visually appear to be close to the impedance vs. frequency behavior of human skin. Our skin phantom’s impedance vs. frequency behavior will be analyzed more in-depth in the proceeding sections.

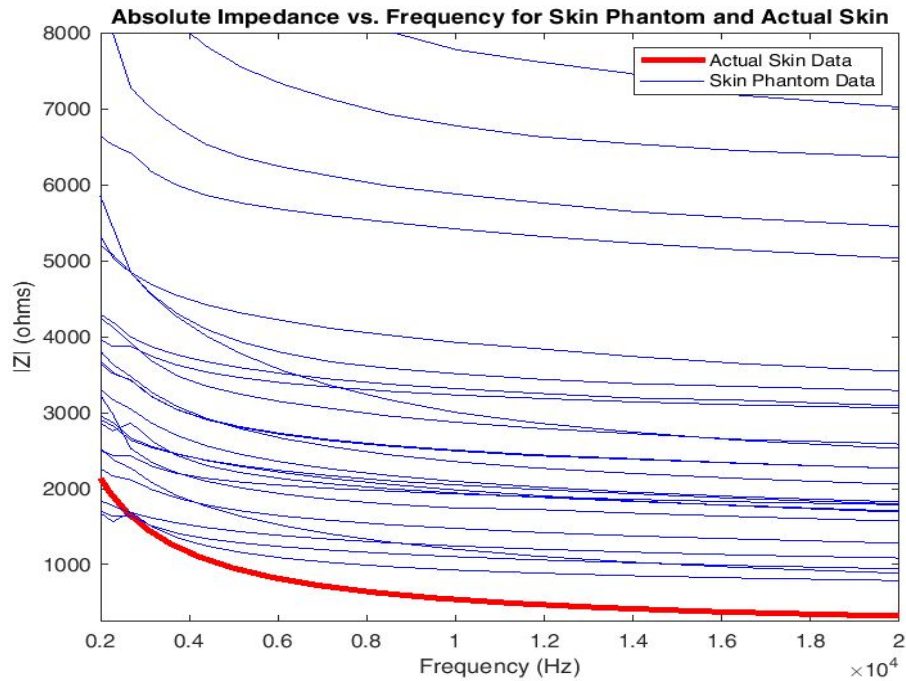


Figure 7.6: Zoomed in Impedance vs. Frequency Curves for Full Factorial Experiment

We noticed during our experimentation that our phantom was not always uniformly wetted on the surface, which perhaps contributed to the higher than average impedance of certain curves seen in Figure 7.5. To test this, we would have liked to rerun the experiment while ensuring that the surface of the phantom was uniformly wetted prior to taking measurements. Unfortunately, due to COVID-19 campus closures, we were unable to complete further physical experimentation. However, this experiment provided a copious amount of data for our analysis.

7.3 Analysis

To reiterate, a full factorial experimental design allows one to understand the effects of each factor on the desired behavior. In this section, we analyzed the effects of each of the four factors on our skin phantom's resistance, capacitance, and overall impedance vs. frequency behavior. We also used the data obtained from the full factorial experiment to create a mathematical model that can predict how close our skin phantom will match the impedance vs. frequency behavior of human skin with inputs of factor levels.

7.3.1 Effects of Factors on Resistance

In order to understand how the four different factors affected resistance, we calculated the average resistance for each of the thirty-two datasets. This was plotted below in Figure 7.7. Each circle represents one dataset.

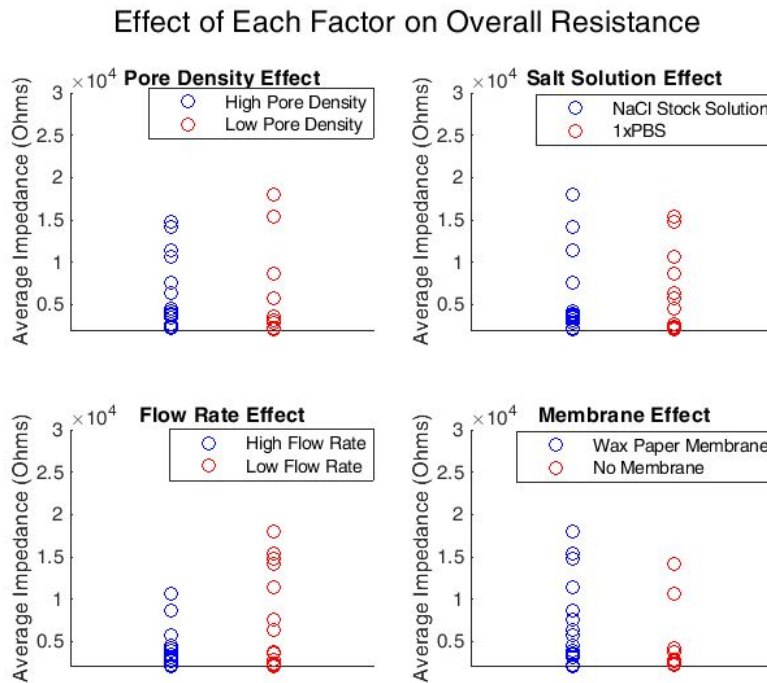


Figure 7.7: Effect of Each Factor on Overall Resistance

Figure 7.7 demonstrates how each factor affected the overall resistance. The plot for the pore density effect shows that the high pore density cases have a slightly lower resistance than the low pore density cases. This suggests that increasing the pore density will slightly decrease the overall resistance of the phantom, as expected.

The plot for the salt solution effect shows that the high salt concentration cases (NaCl stock solution) are clustered at a lower resistance than the low salt solution cases. This suggests that increasing salt concentration decreases the resistance, as we predicted.

The plot for the flow rate effect shows that the high flow rate cases have lower resistance values than the low flow rate cases. This suggests that as we increase the flow rate, our phantom's resistance will decrease, as we predicted.

The plot for the membrane effect shows that cases with a nonpermeable, wax paper membrane have very varied resistance values; the cases without a membrane have very uniform resistance values clustered together at a lower value. This suggests that adding a membrane increases resistance, and also increases variability in our results. This is undesired behavior as increased variability means low repeatability of experiments.

7.3.2 Effects of Factors on Capacitance

In order to understand how each factor affects the capacitance of our skin phantom, we calculated the change in absolute impedance over the change in frequency. Higher capacitances would show a greater decrease in resistance as frequency increases, and lower capacitances would show a smaller decrease in resistance as frequency increases.

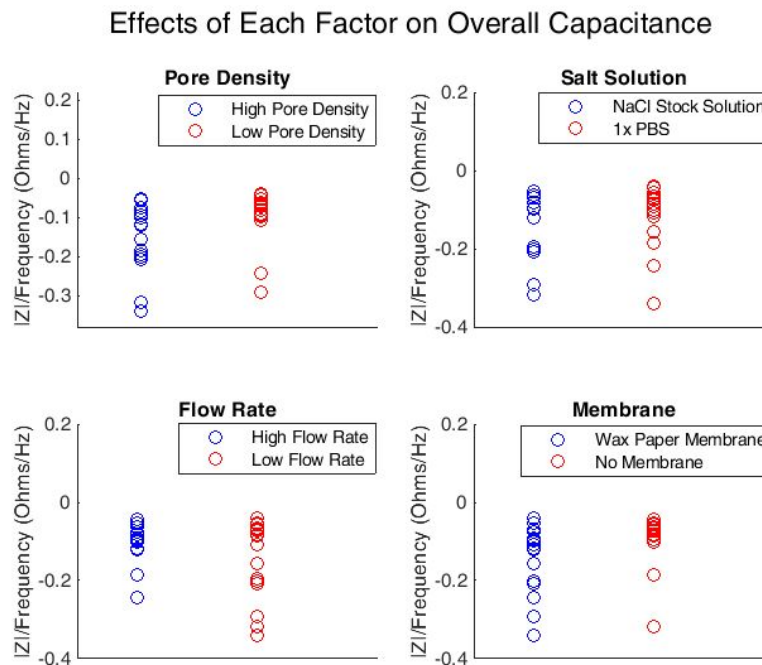


Figure 7.8: Effect of Each Factor on Overall Capacitance

Figure 7.8 demonstrates how each factor affected our skin phantom's capacitance. The plot for the pore density effect shows that cases with a high pore density have a slightly larger decrease in impedance over a ten times change in frequency. This suggests that increasing pore density increases the capacitance of our skin phantom.

The plot for the salt solution effect shows that the cases with a high salt concentration are comparable to cases with a low salt concentration. This suggests that changing salt solution concentration has little effect on our skin phantom's capacitance, which agrees with the fact that our salt solutions acted like a resistor.

The plot for the flow rate effect shows that the cases with a high flow rate show a smaller decrease in impedance over a ten times change in frequency, while cases with a lower flow rate demonstrate a larger change in impedance. This suggests that increasing the flow rate decreases capacitance. This is perhaps due to the fact that when there is a higher flow rate, the salt solution more uniformly covers the surface of the phantom.

The plot for the membrane effect shows that the test cases that included a nonpermeable, wax paper membrane were much more variable than cases without a membrane. The wax paper membrane cases overall had a larger decrease in impedance with respect to frequency than the no membrane cases, suggesting that the use of a nonpermeable membrane increases the capacitance of our skin phantom.

7.3.3 Effects of Factors on Overall Impedance vs. Frequency Behavior

To reiterate, our goal was to create a skin phantom that had the same impedance vs. frequency behavior of human skin. While we can visually see that different test cases appeared to match the skin well in Figure 7.9, we needed to quantify how close our phantom actually matched the desired behavior in order to understand each factor's effect.

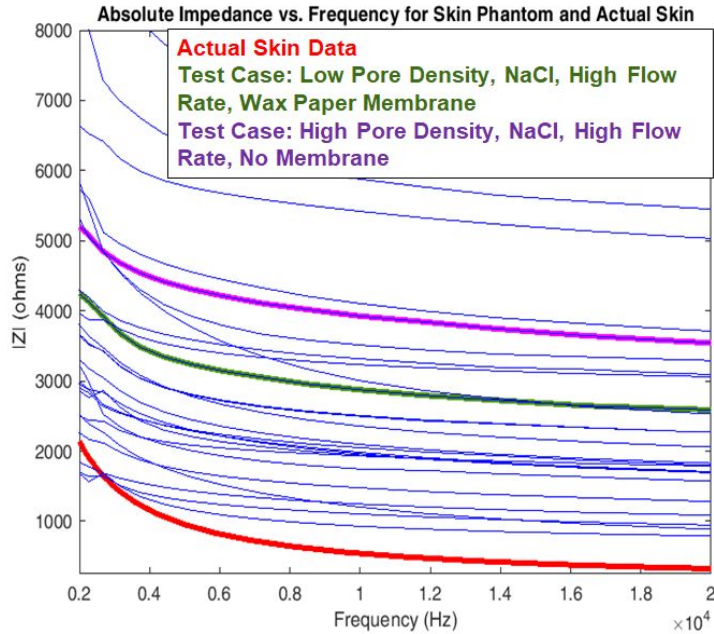


Figure 7.9: Zoomed in Experimental Data with Highlighted Test Cases

We quantified matching impedance vs. frequency behavior by determining a value we call $\Delta\text{Behavior}$. $\Delta\text{Behavior}$ was calculated by subtracting the *in-vivo* skin data from an experimental dataset, then taking the derivative with respect to frequency. The mathematical formula is shown below in Figure 7.10. Values of $\Delta\text{Behavior}$ close to 0 indicate that our skin phantom was a good match for human skin's impedance vs. frequency behavior.

$$\text{Measure of Impedance vs. Frequency Behavior} = \Delta\text{Behavior} = \frac{d|Z|}{df} (\text{Phantom Impedance Data} - \text{Skin Impedance Data})$$

Figure 7.10: Formula for $\Delta\text{Behavior}$

We calculated $\Delta\text{Behavior}$ values for all thirty-two data sets; they are plotted below in Figure 7.11; each dataset's $\Delta\text{Behavior}$ value is represented by a circle.

Effect of Each Factor on Impedance vs. Frequency Behavior

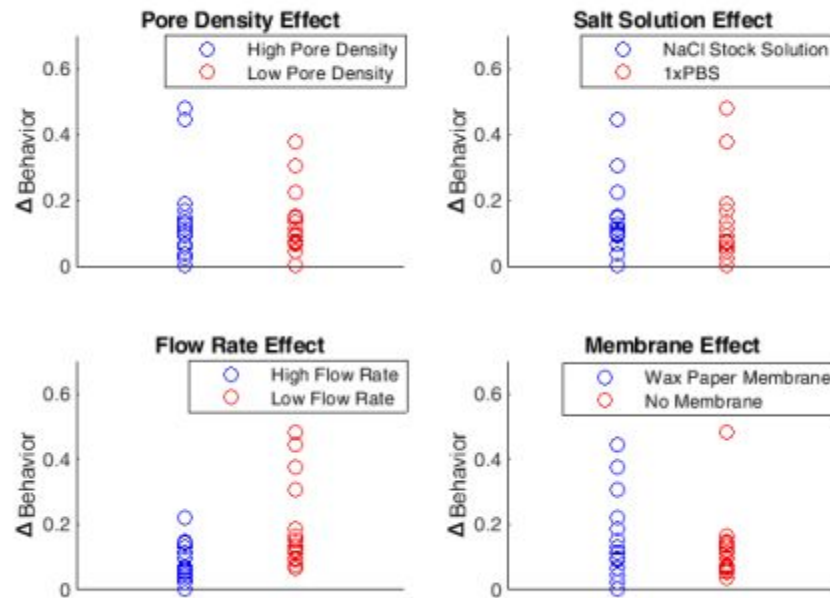


Figure 7.11: Effect of Each Factor on Δ Behavior

Figure 7.11 demonstrates the effect of each factor on our skin phantom's impedance vs. frequency behavior. The plot for the pore density effect shows that cases with high pore density are similar to cases with low pore density. Low pore density cases have slightly lower Δ Behavior values overall, however, the difference is minimal. This suggests that pore density has little overall effect on our phantom's impedance vs. frequency behavior.

The plot for the salt solution concentration-effect shows that cases with a higher salt solution are extremely similar to cases with a low salt solution. This suggests that the salt solution concentration has virtually no effect on our phantom's impedance vs. frequency behavior.

The plot for the flow rate effect shows that cases with a high flow rate have much smaller Δ Behavior values than the cases with a low flow rate. This suggests that increasing the flow rate improves our skin phantom's impedance vs. frequency behavior, making it a better match for human skin.

The plot for the membrane effect shows that cases with a nonpermeable wax paper membrane are, again, highly variable in $\Delta\text{Behavior}$ values. Cases with a membrane have higher $\Delta\text{Behavior}$ values overall compared to cases without a membrane. This suggests that adding a membrane is detrimental to our skin phantom's impedance vs. frequency behavior.

7.3.4 Mathematical Model for $\Delta\text{Behavior}$

Using the thirty-two datasets for our skin phantom, we were able to create a mathematical model through linear regression that would predict a $\Delta\text{Behavior}$ value given an input of the factor levels. The model's equation and associated variables are shown in Appendix A.

We plugged the sixteen test conditions that we used for our experiment into this mathematical model to test it; the resulting predictions for $\Delta\text{Behavior}$ are plotted below in Figure 7.13 against the actual $\Delta\text{Behavior}$ values obtained from our experiment.

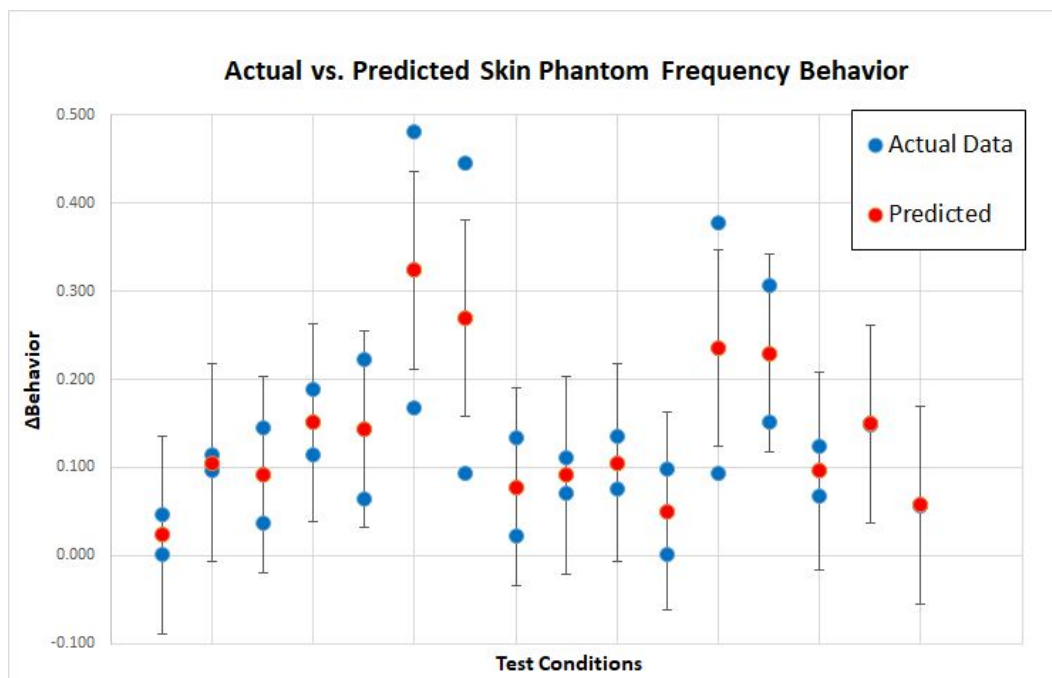


Figure 7.13: Model Predictions for $\Delta\text{Behavior}$ Against Actual $\Delta\text{Behavior}$ Values

The model successfully predicts most of the Δ Behavior values within its error range but fails with cases demonstrating low repeatability. The low repeatability in our experimental data for those three cases where the model fails could have been due to inconsistent wetting on the surface of the phantom or other experimental errors. Repeating the experiment and obtaining more replicates would aid the mathematical model, decreasing its standard error and increasing the accuracy of predictions.

We used the mathematical model to predict for a test case that would give us a Δ Behavior value of $0 \pm .11198$. The model output the factor levels that are shown in Figure 7.14.

Factor:	Level:
Pore Density	1 pore / 5 mm
Salt Solution Concentration	154 mmol
Flow Rate	46.9 μ g/min
Membrane	None

Figure 7.14: Mathematical Model Prediction for Δ Behavior = $0 \pm .11198$

It is important to note that the flow rate level predicted in Figure 7.14 is an extrapolation, as it is outside the range of flow rates that we tested. Thus, this prediction is a place to start further testing rather than a concrete solution. It would be beneficial to run the experiment again using a wider range of flow rates.

8. Professional Engineering Standards and Realistic Constraints

As engineers, there are several standards that always need to be considered when innovating, including ethical, health and safety, sustainability, environmental, regulatory, and manufacturing standards. These standards are known as professional engineering standards. Additionally, there are other constraints, such as budget and time, that are known as realistic constraints. Over the course of this project, we kept all of these standards and constraints in mind.

8.1 The Ethical Justification of Skin Phantoms

Ethical concerns were a primary consideration of this project that influenced many of our decisions. This section of the report will analyze the ethical justification of our project. As mentioned in the Introduction chapter of this thesis, current methods of medical device testing include testing on animal, human, and cadaver subjects. There are many aspects of this kind of testing that raise the question, is this type of testing ethical? One lens with which to analyze this question is through the lens of utilitarianism; utilitarianism is an ethical framework that asserts that the ethical action to take is the one that causes the most happiness and reduces the most harm possible. To apply this lens in the case of skin phantoms, we will compare the harms and happiness caused by using skin phantoms to the harms and happiness caused by alternative options.

As mentioned previously, early-stage medical device tests are typically performed on animals to examine the interactions between the device and the animal; oftentimes, this process is harmful to the animal, causing pain, injury, illness, or death. Once a device has completed animal testing, it goes into clinical testing, where it is then tested on humans. Since there is variation between human and animal physiology, there is still the possibility of harm to human test subjects even if the device was not harmful to animal subjects by the end of preclinical studies. These tests are significant factors of harm and need to be considered when analyzing the medical device industry. However, the medical devices developed from these processes help treat and cure disease states, overall reducing the amount of human pain and suffering. These medical devices are a significant reducer of harms, so it would not be an ethical decision to stop producing them.

Producing medical devices without sufficient testing would also be unethical, as marketing untested, unregulated, and dangerous devices would also cause significant harm.

At the moment, the current medical device testing process is the most ethical; however, that does not mean it cannot be improved. Our team firmly believes that if we can reduce the harms caused by medical device testing while still ensuring the safety of patients using those devices, it is our ethical obligation to do so. While eliminating testing on live subjects is not feasible, the use of skin phantoms would decrease the amount of *in-vivo* testing required, reducing the amount of harm that the medical device industry causes. Thus, the development and utilization of accurate skin phantoms are both ethical actions.

8.2 Health and Safety Implications

There were three health and safety aspects that we kept in mind throughout the duration of this project. We had to ensure that our team was safe during testing, that the end-user would be safe when using our skin phantom, and that any patients using a device that was tested on a completed skin phantom would be safe.

To ensure our own safety, we developed certain protocols during fabrication and testing. To begin with, we chose materials to work with that were not dangerous to us: PDMS, carbon black, and NaCl solutions. During fabrication, we wore gloves, safety glasses, and lab coats, and worked in the hood when desiccating. During testing, the primary hazard was electrocution from the potentiostat. To minimize that danger, we kept the current at 1 mA, a level not dangerous to us. We also ensured that no one actually touched the potentiostat while it was running.

Our material choices also ensured that the end-user would also be safe. Cured PDMS and carbon black are non-toxic and non-hazardous. NaCl solution is also incredibly safe, and can actually be disposed of down the drain. The end-user would not be using a potentiostat; instead, they'd be placing their biowearable onto our phantom. Thus, there would be no danger from our phantom to the end-user.

Our final concern was for any patient or test subject that would use a biowearable tested on our phantom. While the patient or test subject would have no interaction with our phantom, if our phantom malfunctioned in any way during the testing, it could mean the biowearable isn't actually safe for use. Hence, we would be very strict on when our phantom could actually be used; our phantom should only be used to test for signal acquisition or emittance and is not a suitable test for other properties. Additionally, our phantom is not yet ready for testing biowearables. We would want our phantom to be much more accurate and undergo many more tests before it could possibly be used for testing a biowearable.

8.3 Sustainability as a Constraint

Sustainability, or the ability to maintain the use of resources in a way that avoids depletion, is an important constraint for modern innovators. We wanted to design a phantom that produced as little waste as possible and that could withstand many tests in order to decrease the number of resources needed for production. We chose to use PDMS for its stability and low degree of degradation over time [17, 18]. While we were unable to complete fatigue testing on our completed phantoms, each phantom remained in perfect shape after more than sixteen tests. We estimate that our phantoms would remain in usable shape for at least fifty tests, though an experiment would need to be done to validate that. Thus, we successfully created a skin phantom that was reusable.

8.4 Civic Engagement and Compliance with Regulations

As the medical device industry is heavily regulated, it is important that any innovations pertaining to the medical device field also be compliant with those regulations. While we designed our skin phantom to be an alternative early-stage testing method for biowearables, we do not advocate for our phantom to completely supplant current testing methods. Biowearable companies should still comply with federal regulations regarding the necessary testing of medical devices. Our device is only intended to be used to replace or supplement early testing so that when biowearables are eventually tested on a live subject, it is more likely to be successful. In the future, it would be ideal to replace certain animal and human trials with skin phantom

trials, but we acknowledge that the technology is not there yet. All biowearable testing should be compliant with the appropriate federal regulations.

8.5 Manufacturability

Manufacturability is a concern for any kind of innovation. We broke down our manufacturability goals into short- and long-term goals. Our short term manufacturability goals pertained to how easy it was for us to fabricate the phantoms in our lab. We took steps to use easily acquirable materials and disposables. We decided to use the Cricut machine to cut channels as opposed to using photolithography as we wanted to be able to iterate our design efficiently. Photomasks are costly and take time to produce and ship. We also mixed the PDMS by hand in disposable plastic cups. Thus, the most complicated part of manufacturing our phantoms was the plasma bonding step.

For a long term manufacturing process, however, we would change the process to be more easily scaled up. We would recommend the use of more commercialized PDMS fabrication techniques. Photolithography could be used to pattern multiple PDMS layers at once, speeding up the process. Additionally, using a centrifugal mixer would allow for larger quantities of PDMS and carbon black-doped PDMS to be made at once. Our design was made in such a way that it would be possible to scale up production in this way. Even if a biowearables company did not have access to a plasma oven or photolithography equipment, the production of the phantoms could be outsourced to a lab. Some labs even rent out their microfluidic and photolithography lab spaces for commercial use.

8.6 Budget Constraints

The budget is a constraint that needs to be considered for any project. Our project was funded by the Santa Clara University School of Engineering. We were given \$2000 to purchase equipment and materials. While our anticipated cost was \$2,000, we ended up only spending \$658.35. A detailed funding request and an actual spending list are located in Appendix B. Had we needed to

purchase or rent a potentiostat, that would have been a significant cost. However, Proteus Digital Health generously allowed us the use of his potentiostat.

8.7 Time Constraints

As this was a year-long thesis project, we had to plan ahead to ensure we would complete the project in three quarters. Our original plan can be seen in Appendix C.1. However, we had significant purchasing delays at the beginning of the second quarter, which pushed our prototyping and testing out by four weeks. Additionally, the campus closure due to COVID-19 during week 10 of the second quarter cut off our physical testing and prototyping early. However, even with the unexpected loss of experimentation time, we were able to perform significant analyses on data we already collected. Our actual timeline can be seen in Appendix C.2.

9. Summary and Conclusion

9.1: Summary of the Project

In order to meet the biowearable industry's need for a new testing method, we developed a skin phantom that emulated human skin's perspiration mechanism and corresponding impedance vs. frequency spectrum. Our skin phantom met our desired goals of matching the impedance vs. frequency behavior of skin from 2,000 - 20,000 Hz, while also being sustainable, safe, and easily manufacturable. We also succeeded in creating models and simulations that characterized our materials and aided in our understanding of our skin phantom.

9.2: Future Work

While we successfully met our goals for our project this year, there are further improvements that need to be made to our phantom. In the future, movement capabilities need to be added to our skin phantom. The movement of skin has been known to affect a biowearable's function due to changes in electrical contact. As our phantom is made of an elastomer, variations in the amount of crosslinker used can alter its stretchability. Usage of motors or an inflatable bladder can simulate movements due to breathing and stretching.

Future teams should also build the memristor circuit model we developed to ensure it works the way as designed and accurately mimics the nonlinear electrical behavior of skin. Future teams carrying on this project should work to simulate more complex geometry in CST. Being able to completely simulate our phantom would allow for factor testing through simulation, which will make benchtop testing more efficient. Accurately characterizing the electrical properties of our specific materials will aid in creating an accurate CST model, and should be done by the incoming team.

Finally, before our phantom can be used to test biowearables, many more replicates of the full factorial test need to be run. This will ensure that our phantom gives repeatable data, and will also improve our mathematical model to be more accurate. Further testing should also increase the range of flow rates and salt solution concentrations tested to get a broader view of how those

factors affect our phantom's behavior. Other testing that needs to be done includes testing durability, the effect of different kinds and sizes of electrodes, and the effect of environmental changes (such as temperature and humidity).

9.3: Lessons Learned

There were two critical lessons we learned during this project. The first was the importance of experimental design; had we not planned out our experiment in an efficient way, we would not have had enough data to analyze after the campus closed down. Using Design of Experiments methods allowed us to design a full factorial experiment that provided us many different kinds of information on our phantom. Even with the campus closure and the end of physical experiments, the Design of Experiments methods ensured that we had enough data to finish our project.

This leads to our second lesson learned: being able to pivot when there are unexpected setbacks. Due to an unexpected purchasing setback and the COVID-19 campus closures, our prototyping and testing periods were limited to only five weeks. By quickly shifting our focus to planning, statistical analysis, and simulations, we were still able to meet our initial goals.

10. Sources Cited

- [1] Dias, D., & Paulo Silva Cunha, J. (2018). Wearable Health Devices-Vital Sign Monitoring, Systems and Technologies. *Sensors (Basel, Switzerland)*, 18(8), 2414. <https://doi.org/10.3390/s18082414>
- [2] Cappon, G., Vettoretti, M., Sparacino, G., & Facchinetti, A. (2019). Continuous Glucose Monitoring Sensors for Diabetes Management: A Review of Technologies and Applications. *Diabetes & metabolism journal*, 43(4), 383–397. <https://doi.org/10.4093/dmj.2019.0121>
- [3] Proteus Digital Health (2014). Proteus Patch With Ingestible Sensor Accessory: Instructions For Use. <https://www.proteus.com/wp-content/uploads/2015/05/LBL-0171-Rev-2-Global-CMD-Dw5-IFU.pdf>
- [4] Proteus Digital Health (2019). “Proteus Digital Health: Evidence”. <https://www.proteus.com/evidence/>
- [5] Sall B. Regulation of Medical Devices. In: Madame Curie Bioscience Database [Internet]. *Austin (TX): Landes Bioscience; 2000-2013*. Available from: <https://www.ncbi.nlm.nih.gov/books/NBK6534/>
- [6] Dąbrowska, K., Rotaru, G., Derler, S., Spano, F., Camenzind, M., Annaheim, S., & Rossi, R. M. (2016). Materials used to simulate physical properties of human skin. *Skin Research and Technology*, 22(1), 3-14. doi:10.1111/srt.12235
- [7] National Academy Press. (1996). Criteria for Selecting Experimental Animals. In *Laboratory Animal Management: Rodents* (pp. 16–20). Washington D.C.
- [8] Rovida, C., & Hartung, T. (2009). Re-evaluation of animal numbers and costs for in vivo tests to accomplish REACH legislation requirements for chemicals - a report by the transatlantic think tank for toxicology (t(4)). *ALTEX*, 26(3), 187–208.
- [9] Lawrence, W., Jr. (1993). Patient selection for clinical trials. risks versus benefits and quality of life issues. *Cancer*, 72(9 Suppl), 2798-2800. doi:10.1002/1097-0142(19931101)72:9+<2798::aid-cncr2820721504>3.0.co;2-# [doi]

- [10] EwonuBari, E., Jacks, T., Amaza, D. S., Nwegbu, M., Abue, A., & Effiong, O. (2012). Problems and prospects of acquisition of human cadaver for medical education in Nigeria. *JPMA.the Journal of the Pakistan Medical Association*, 62, 1134-6.
- [11] Akhtar A. (2015). The flaws and human harms of animal experimentation. *Cambridge quarterly of healthcare ethics : CQ : the international journal of healthcare ethics committees*, 24(4), 407–419. <https://doi.org/10.1017/S0963180115000079>
- [12] Habicht, J. L., Kiessling, C., & Winkelmann, A. (2018). Bodies for Anatomy Education in Medical Schools: An Overview of the Sources of Cadavers Worldwide. *Academic medicine : journal of the Association of American Medical Colleges*, 93(9), 1293–1300. <https://doi.org/10.1097/ACM.0000000000002227>
- [13] Liu, C., Huang, Y., Li, S. Chen, Y., Wang, W. Z., Yu, J., & Shih W. (2019). *Microelectromechanical system-based biocompatible artificial skin phantoms* doi:10.1049/mnl.2018.5112
- [14] Pinto, A. M. R., Bertemes-Filho, P., & Paterno, A. (2015). Gelatin: A skin phantom for bioimpedance spectroscopy. *Biomedical Physics & Engineering Express*, 1(3), 035001. doi:10.1088/2057-1976/1/3/035001
- [15] Fischer M. H. (1905). The Toxic Effects Of Formaldehyde And Formalin. *The Journal of experimental medicine*, 6(4-6), 487–518. <https://doi.org/10.1084/jem.6.4-6.487>
- [16] Dalev, P., Vassileva, E., Mark, J., & Fakirov, S. (1998). Enzymatic degradation of formaldehyde-crosslinked gelatin. *Biotechnology Techniques - Biotechnol Technique*, 12, 889-892. doi:10.1023/A:1008861411364
- [17] Ruhhammer, J., Zens, M., Goldschmidtboeing, F., Seifert, A., & Woias, P. (2015). Highly elastic conductive polymeric MEMS. *Science and Technology of Advanced Materials*, 16(1), 015003. doi:10.1088/1468-6996/16/1/015003 [doi]
- [18] Rocha, R., & Tavakoli, M. (2017). Carbon doped PDMS: Conductance stability over time and implications on additive manufacturing of stretchable electronics. *Journal of Micromechanics and Microengineering*, 27 doi:10.1088/1361-6439/aa5ab1

- [19] Belanger, M. C., & Marois, Y. (2001). Hemocompatibility, biocompatibility, inflammatory and in vivo studies of primary reference materials low-density polyethylene and polydimethylsiloxane: A review. *Journal of Biomedical Materials Research*, 58(5), 467-477. doi:10.1002/jbm.1043 [pii]
- [20] Subramaniam, A., & Sethuraman, S. (2014). In Kumbar S. G., Laurencin C. T. and Deng M.(Eds.), Chapter 18 - biomedical applications of nondegradable polymers. *Oxford: Elsevier*. doi:https://doi.org/10.1016/B978-0-12-396983-5.00019-3
- [21] Guraliuc, A. R., Zhadobov, M., & Sauleau, R. (2014). PDMS-based skin-equivalent phantom for propagation studies in the 58–63 GHz range doi:10.1109/MOBIHEALTH.2014.7015944
- [22] Garrett, J. & Fear, E. (2014). Stable and flexible materials to mimic the dielectric properties of human soft tissues. *IEEE Antennas and Wireless Propagation Letters*, 13, 599-602. doi:10.1109/LAWP.2014.2312925
- [23] Pabst, O., Martinsen, Ø G., & Chua, L. (2018). The non-linear electrical properties of human skin make it a generic memristor. *Scientific Reports*, 8(1), 15806. doi:10.1038/s41598-018-34059-6
- [24] Baker, L. B. (2017). Sweating rate and sweat sodium concentration in athletes: A review of methodology and intra/interindividual variability. *Sports Medicine* (Auckland, N.Z.), 47(Suppl 1), 111-128. doi:10.1007/s40279-017-0691-5 [doi]
- [25] Fallon, R. H., & Moyer, C. A. (1963). Rates of insensible perspiration through normal, burned, tape stripped, and epidermally denuded living human skin. *Annals of Surgery*, 158(6), 915-923. doi:10.1097/00000658-196312000-00001
- [26] Ohhashi, T., Sakaguchi, M., & Tsuda, T. (1998). Human perspiration measurement. *Physiological Measurement*, 19(4), 449-461. doi:10.1088/0967-3334/19/4/001
- [27] J. Rosell, J. Colominas, P. Riu, R. Pallas-Areny, & J. G. Webster. (1988). Skin impedance from 1 Hz to 1 MHz doi:10.1109/10.4599
- [28] “Potentiostat Fundamentals.” Potentiostat/Galvanostat Electrochemical Instrument Basics, Gamry Instruments, www.gamry.com/application-notes/instrumentation/potentiostat-fundamentals/.
- [29] Simulia. (n.d.). CST Studio Suite 3D EM simulation and analysis software. Retrieved June 02, 2020, from <https://www.3ds.com/products-services/simulia/products/cst-studio-suite/>

Appendix A: Mathematical Model for Predicting Δ Behavior

$$\begin{aligned} \Delta \text{Behavior Predicted} = & 0.13750 + 0.00213 * A - 0.00430 * B - 0.05196 * C + 0.01002 * D + \\ & 0.01714 * A * B - 0.01853 * A * C - 0.01261 * A * D - 0.01877 * B * C - 0.02130 * B * D - \\ & 0.02180 * C * D + 0.00424 * A * B * C - 0.01426 * A * B * D + 0.01915 * A * C * D + \\ & 0.02128 * B * C * D + 0.02977 * A * B * C * D \end{aligned}$$

Where:

A: 1 for High Pore Density, -1 for Low Pore Density

B: Salt Solution Concentration normalized between -1 and 1, where 1 is 154 mmol and -1 is 137 mmol

C: Flow Rate normalized between -1 and 1, where 1 is 14.2 $\mu\text{g}/\text{min}$ and -1 is 9.18 $\mu\text{g}/\text{min}$

D: 1 for nonpermeable, wax paper membrane, and -1 is no membrane

Standard Error = .11198

Appendix B: Budget and Actual Spending

B.1 Proposed Budget:

Material	Cost per unit (\$)	Units desired	Total Cost (\$)
Synthetic Skin Layer			
Hydrogel	200	1	200
Cosmetic Puff (x10)	2	10	20
Photoresist	150	1	150
PDMS (Sylgard-184)	128.39	2	256.78
Fumasep FAS-30	16	10	160
Fabrication & Safe Handling			
Masks	200	1	200
Ionic/Conductive Solutions			
Artificial Sweat	164.84	1	164.84
NaCl Solution	24.95	2	49.9
Electrical Components			
Memristor (Discovery Kit)	489	1	489
Memristor (SDC Carbon)	89	1	89
Resistors Kit	50	1	50
Solder Spool	25	1	25
30 Gauge Wire Kit	15.95	1	15.95

Snap Electrodes	12.99	6	77.94
Cables	60	4	180
Measurement of Electrical Characteristics			
Circuit components to build a potentiostat – (2 op amps, 1 resistor, 3 electrodes)	1	1	45
Breadboard	5	5.5	27.5
Printed Circuit Board Fabrication	1	1	100
Tools to Change and Measure Changeable Physical Characteristics of Phantom			
Thermometer (humidity)	6	1	6
Chamber to control humidity	25.25	1	25.24
Conductive Materials			
Carbon black	25	2	50
Miscellaneous			
Petri Dishes	12.3	2	24.6
Copper tape	6	2	12
Electrical Tape	1	1	10

junction box	1	1	25.5
Silicon Wafers x4	15	4	60
Total			2514.25

B.2 Purchase Record:

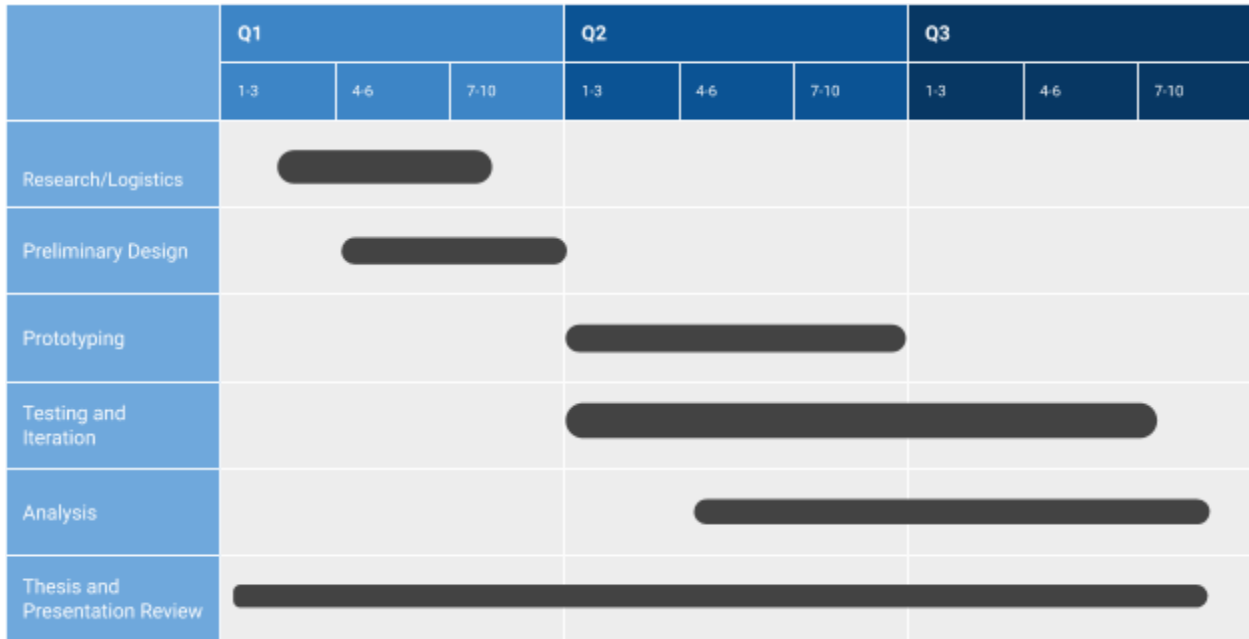
Item	Unit Size	Quantity	Cost	Link
Plastic Bin	1	1	16.99	https://www.amazon.com/Anbers-Quart-Plastic-Latching-Handles/dp/B07T2Q2PRO/ref=sr_1_7?keywords=plastic+bin+with+lid&qid=1578517416&sr=8-7
10mL Luer Lock Syringe	100	1	13.49	https://www.amazon.com/10ml-Syringe-Sterile-BH-SUPPLIES/dp/B07KW4KLG2/ref=sr_1_3?keywords=luer+lock+syringe+10ml&qid=1578518073&sr=8-3
Petri Dish w/ Pipettes	20	1	12.35	https://www.amazon.com/Sterile-Transfer-Pipettes-10Pcs3ml-10Pcs2ml/dp/B07MZ8CXHY/ref=sr_1_3?keywords=sterile+petri+dishe&qid=1578690313&sr=8-3
Tygon Microbore tubing	1	1	60.73	https://www.coleparmer.com/i/tygon-microbore-tubing-0-020-x-0-060-od-100-ft-roll/0641901
20gax0.5" Dispensing Tip	50	1	9.50	https://www.cmlsupply.com/dispensing-needle-20ga-0-5-tip-yellow/
21gax0.5" Dispensing Tips	50	1	9.50	https://www.cmlsupply.com/dispensing-needle-21ga-0-5-tip-green/
Metal Electrode: Set of 11	11	1	29.00	https://sciencekitstore.com/metal-electrodes-set-of-11/?gclid=CjwKCAiAu9vwBRAEEiwAzvjq-8VLS2uhAjc_ZbzCoojQfGPhZudcpQt1e1iHRfqdy73DVJW91iXRphoC1jYQAvD_BwE

Sylgard 184 (PDMS)	1	2	266.00	https://www.amazon.com/Sylgard-Solar-Encapsulation-Making-Panels/dp/B004IJENBG/ref=sr_1_1?gclid=EAIaIQobChMIoIOhq6735gIVhcJkCh2TiguNEAAYAiAAEgIFffD_BwE&hvadid=176366437624&hvdev=c&hvlocphy=9032151&hvnetw=g&hvpos=1t2&hvqmt=e&hvrnd=3334184446896095109&hvtargid=kwd-19326695247&hydadcr=25238_9775703&keywords=sylgard+184&qid=1578601932&sr=8-1&th=1
Carbon Black - Vulcan XC 72	1	1	50.00	https://www.fuelcellstore.com/vulcan-xc72
Carbon Black - Vulcan XC 72R	1	1	50.00	https://www.fuelcellstore.com/vulcan-xc-72r?search=72r
Fumasep FAS-30	1	5	80.00	https://www.fuelcellstore.com/fumasep-fas-30
Sodium Chloride, 0.9% w/v, Standards and Solutions, Bottle, 500mL	1	1	14.66	https://www.grainger.com/product/LABCHEM-Sodium-Chloride-8GE79
Cricut Replacement Cutting Blades for Cutting Machines	2	1	7.38	https://www.amazon.com/Cricut-Replacement-Cutting-Blades-Machines/dp/B000XANNVA/ref=asc_df_B000XANNVA/?hvadid=194970149026&hvdev=c&hvdvcmld=&hvlocint=&hvlocphy=9032151&hvnetw=g&hvponc=&hvpos=1o1&hvptwo=&hvqmt=&hvrnd=1123901514633206814&hvtargid=pla-311427768403&linkCode=df0&tag=hyprod-20&th=1

Deep Cut Blades for Cricut Explore Air 2,10 Pieces 60 Degree Cutting Replacement Blades for Cricut Explore Air Air 2 Maker with Anti Lost Bag and Storage Container	10	1	8.99	https://www.amazon.com/Blades-Explore-Cutting-Machines-Replacement/dp/B07FZXWN2F/ref=sr_1_10?crid=3BCGY63CSQKCZ&keywords=cricut+explore+deep+cut+blade&qid=1581546587&s=arts-crafts&srefix=cricut+explore+deep%252Carts-crafts%252C207&sr=1-10
Coil Shim Stock – 316 Stainless Steel	1	1	29.76	https://www.maudlinproducts.com/shim-products/coil-shim-stock/coil-shim-stock-316-stainless-steel/
		Total:	658.35	

Appendix C: Timeline

C.1 Original Proposed Timeline



C.2 Actual Timeline Due to Purchasing Delays/COVID-19 Campus Closure

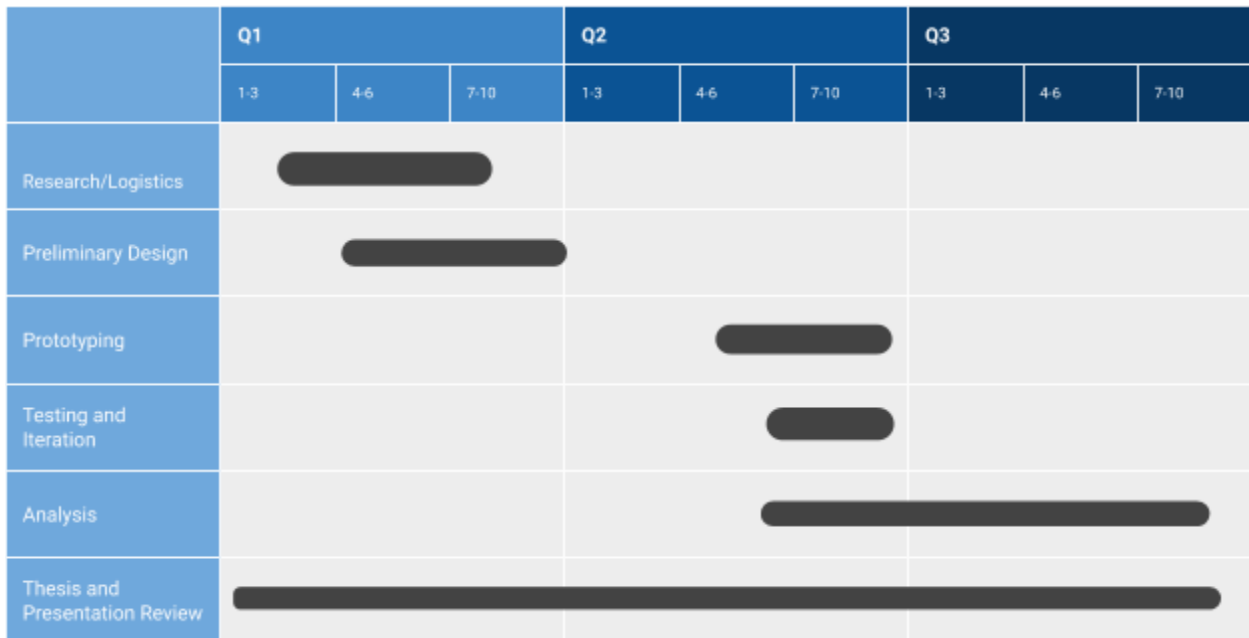


Table of Contents

	Page
Abstract.....	iii
Acknowledgments.....	iv
Chapter 1: Project Introduction.....	1
1.1: Project Rationale.....	1
1.1.1: Problems with Current Bio-Wearable Testing Methods.....	2
1.2: Skin Phantoms.....	4
1.2.1: Existing Skin Phantoms.....	5
1.2.2: Market Needs Analysis.....	6
1.2.3: Skin Phantoms that Mimic Electrical Properties of Skin.....	7
1.2.4: Physiology of Human Skin Contributing to Impedance.....	8
1.3 Project Goal.....	11
Chapter 2: The Skin Phantom System.....	12
2.1: System Overview.....	12
2.1.1: The Physical Model Subsystem.....	13
2.1.2: The Electrical Data Collection Subsystem.....	13
2.1.3: The Circuit Model.....	13
2.1.4: The Computer Simulated Model.....	13
2.2: Integration of Subsystems.....	14
Chapter 3: Subsystem 1: The Physical Model.....	15
3.1: Overview of Subsystem.....	15
3.2: Material Choice.....	16
3.3: Fabrication.....	17
3.3.1: Flat PDMS Layers.....	18
3.3.2: Carbon Black Doped Base Layer.....	18
3.3.3: Skin Phantom Cutting and Assembly.....	19
3.4: Syringe Pump.....	20
3.4.1: Flow Rate of Salt Solution.....	20
Chapter 4: Subsystem 2: Electrical Data Collection.....	21
4.1: Overview of Subsystem.....	21
4.2: Potentiostat.....	21
4.2.1: Probe System.....	22
4.2.2: Software.....	22
4.3: Initial Testing of Potentiostat.....	23
Chapter 5: Subsystem 3: The Circuit Model.....	25
5.1: Overview of Subsystem.....	25
5.2: Data Provided by Proteus Digital Health.....	25
5.3: Early Circuit Model for Skin.....	26

5.4: Updated Circuit Model.....	27
5.5 Skin & Memristor Properties.....	28
5.6 ADS Model & Simulation.....	29
Chapter 6: Subsystem 4: Computer Simulations of the Skin Phantom.....	32
6.1: Overview of Subsystem.....	32
6.2: Baseline - “Hello World” Test.....	33
6.3 Material Simulations.....	35
6.3.1 CST Skin.....	35
6.3.2 Simplified Model of Skin - Wet Vs. Dry.....	37
6.3.3 Carbon Black + PDMS.....	40
6.3.4 PDMS.....	42
6.3.5 Simplified Model of Skin Phantom.....	43
6.4 Future Work.....	45
Chapter 7: System Integration, Testing, and Analysis.....	47
7.1: Integrating the Physical Model and Electrical Measurement System.....	47
7.1.1: Preliminary Results.....	47
7.2: Full Factorial Experiment.....	49
7.2.1: Experimental Procedure.....	50
7.2.2: Experimental Results.....	51
7.3: Analysis.....	53
7.3.1: Effects of Factors on Resistance.....	54
7.3.2: Effects of Factors on Capacitance.....	55
7.3.3: Effects of Factors on Overall Impedance vs. Frequency Behavior.....	56
7.3.4: Mathematical Model for Δ Behavior.....	59
Chapter 8: Professional Engineering Standards and Realistic Constraints	61
8.1: The Ethical Justification of Skin Phantoms.....	61
8.2: Health and Safety Implications.....	62
8.3: Sustainability as a Constraint.....	63
8.4: Civic Engagement and Compliance with Regulations.....	63
8.5: Manufacturability.....	64
8.6: Budget Constraints.....	64
8.7: Time Constraints.....	65
Chapter 9: Summary and Conclusion.....	66
9.1: Summary of the Project.....	66
9.2: Future Work.....	66
9.3 Lessons Learned.....	67
Chapter 10: Sources Cited.....	68
Appendix A: Mathematical Model for Predicting Δ Behavior.....	71
Appendix B: Budget and Actual Spending.....	72

B.1: Proposed Budget.....	72
B.2: Purchase Record.....	74
Appendix C: Timeline.....	77
C.1: Original Proposed Timeline.....	77
C.2: Actual Timeline Due to Purchasing Delays/COVID-19 Campus Closure.....	77

List of Figures

	Page
Figure 1.1: Materials Used to Simulate Skin Properties.....	5
Figure 1.2: Skin impedance from 1 Hz to 1 MHz.....	10
Figure 1.3: In-Vivo Skin Impedance vs. Frequency from Jim Hutchison.....	10
Figure 2.1: Systems Level Diagram of Skin Phantom.....	12
Figure 3.1: Simplified Perspiration model.....	15
Figure 3.2: Cross Section of Skin Phantom.....	16
Figure 3.3: Overview of Fabrication Process.....	17
Figure 3.4: Carbon Black Layer Fabrication.....	18
Figure 3.5: Bonding and Hole Punching Process.....	19
Figure 3.6: Syringe Pump Connected to the Inlet of Phantom Via Tygon Tubing.....	20
Figure 4.1: Potentiostat Schematic.....	21
Figure 4.2: Test Conditions on IviumSoft.....	23
Figure 4.3: Impedance vs. Frequency for 10 kOhm Resistor.....	24
Figure 5.1: In-Vivo Skin Impedance vs. Frequency Data from Proteus Digital Health.....	25
Figure 5.2: First Circuit Model for Skin.....	26
Figure 5.3: Simple Skin Equivalent Circuit Model from Proteus Digital Health.....	26
Figure 5.4: Impedance vs. Frequency for Simple Skin Equivalent Model.....	27
Figure 5.5: Updated Circuit Model for Skin.....	28
Figure 5.6: ADS Memristor Circuit.....	30
Figure 5.7: VSUM Node Equation.....	30
Figure 5.8: VINT Node Equation.....	30
Figure 5.9: VZ Node Equation.....	30
Figure 5.10: Memristor Hysteresis Loop.....	31
Figure 6.1: Silicon Dioxide Capacitor Simulation.....	33
Figure 6.2: Capacitance of Silicon Capacitor.....	34
Figure 6.3 : Graph of $\frac{1}{j\omega c}$	35
Figure 6.4: Bio Tissue for Bio Tissue/Skin.....	36
Figure 6.5: Impedance Vs. Frequency of Bio/Tissue Skin.....	37
Figure 6.6: Dry Skin 1mmx1mm, Fat 1mmx3mm, Muscle 1mmx5mm.....	38
Figure 6.7: Impedance Vs. Frequency of Simplified Skin Model - Dry.....	38
Figure 6.8: Wet Skin 1mmx1mm, Fat 1mmx3mm, Muscle 1mmx5mm.....	39
Figure 6.9: Impedance Vs. Frequency of Simplified Skin Model - Wet.....	39
Figure 6.10: Carbon Black + PDMS Sample With Discrete Port and PEC sheets.....	41
Figure 6.11: Impedance Vs. Frequency Graph of Carbon Black + PDMS.....	42
Figure 6.12: PDMS Sample With Discrete Port and PEC sheets.....	42
Figure 6.13: Impedance VS. Frequency Graph of PDMS.....	43
Figure 6.14: Simplified Skin Phantom Model.....	44
Figure 6.15: Real/ Imaginary Components of Impedance Vs. Frequency of Simplified Circuit.....	44
Figure 6.16: CST Model of Actual Skin Phantom.....	45
Figure 7.1: Integration of Physical Model and Electrical Measurement System.....	47
Figure 7.2: Impedance vs. Frequency for Thick and Thin Carbon Black Layers and Skin.....	48

Figure 7.3: Impedance vs. Frequency for Different Salt Solutions.....	49
Figure 7.4: Levels for Each Factor in Full Factorial Experiment.....	50
Figure 7.5: Impedance vs. Frequency for In-Vivo Skin and 32 Skin Phantom Datasets.....	52
Figure 7.6: Zoomed in Impedance vs. Frequency Curves for Full Factorial Experiment.....	53
Figure 7.7: Effect of Each Factor on Overall Resistance.....	54
Figure 7.8: Effect of Each Factor on Overall Capacitance.....	55
Figure 7.9: Zoomed in Experimental Data with Highlighted Test Cases.....	57
Figure 7.10: Formula for Δ Behavior.....	57
Figure 7.11: Effect of Each Factor on Δ Behavior.....	58
Figure 7.12: Mathematical Model for Δ Behavior.....	59
Figure 7.13: Model Predictions for Δ Behavior Against Actual Δ Behavior Values.....	60

List of Tables

	Page
Table 5.1: Skin & Memristor Properties.....	29
Table 6.1: Material Properties of Materials used in CST Simulations.....	36